Zhang *et al.*
Cell Communication and Signaling (2025) 23:138
https://doi.org/10.1186/s12964-025-02134-x

Cell Communication and Signaling

RESEARCH

Open Access

PLZF-expressing CD4$^+$ T cells promote tissue-resident memory T cells in breaking immune tolerance in allergic asthma via IL-15/IL-15Rα signaling

Meng Zhang[1], Sheng-ce Tao[2,3], Na Li[4], Jingjing Feng[1], Tianyun Shi[1], Yunxia Yu[1], Xiaoting Ren[1], Jiafeng Sha[1], Zhoufang Mei[1] and Zhijun Jie[1,5*]

Abstract

Background Allergic asthma is a chronic airway disease characterized by an allergic response and altered immune tolerance. CD4$^+$ tissue-resident memory T (TRM) cells are crucial in the chronic and relapsing pathogenesis of asthma. Furthermore, promyelocytic leukemia zinc finger (PLZF) is an essential transcription factor involved in asthmatic tolerance and has been implicated in the regulation of CD4$^+$CD44$^+$ memory T cells. However, the role of CD4$^+$ TRM cells in asthmatic tolerance, as well as their potential modulation by PLZF, remain unclear. Therefore, in the current study, we explore the role of CD4$^+$ TRM cells in asthmatic immune tolerance and as well as the regulatory role of PLZF in this process.

Methods To elucidate the role of CD4$^+$ TRM cells in immune tolerance, asthma memory mouse models were treated with the immunomodulator FTY720. Subsequently, CD4$^+$ T cells were isolated from the lungs and spleens and transferred to oral tolerance mouse models. To explore the regulation of PLZF in CD4$^+$ TRM cells, asthma and oral tolerance were established in Zbtb16$^{flox/flox}$ CD4^{Cre} and wild-type mice. Flow cytometry, histological analysis, and cytokine measurements were performed to characterize the immune response. The regulatory activity of PLZF on CD4$^+$ TRM cells was analyzed through quantitative proteomics and verified in vitro and vivo.

Results The CD4$^+$ TRM cell proportion positively correlated with the pathological phenotypes and molecular characteristics of asthma. Adoptive transfer of CD4$^+$ TRM cells induced asthmatic phenotypes. This suggested that CD4$^+$ TRM cells contributed to the pathogenesis of asthma. Conditional knockout of PLZF substantially reduced the proportion of CD4$^+$ TRM cells, relieved asthmatic symptoms, and suppressed the interleukin (IL)-15/IL-15Rα signaling pathway. Furthermore, exposure to the IL-15Rα agonist restored asthma-related Th2 inflammation, accompanied by a markedly increased proportion of CD4$^+$ TRM cells. Meanwhile, IL-15 and ovalbumin(OVA)-primed Beas2b supernatant co-stimulation in vitro enhanced the differentiation of pulmonary PLZF-expressing CD4$^+$ T cells into CD4$^+$ TRM cells.

Conclusions This study identified CD4$^+$ TRM cells as key mediators of immune tolerance in asthma. This process is regulated by the transcription factor PLZF in CD4$^+$ T cells through IL-15/IL-15Rα signaling. Thus, targeting PLZF or the IL-15/IL-15Rα pathway may represent a promising therapeutic strategy for treating asthma.

Keywords Asthma, Oral tolerance, Immune memory, PLZF, Tissue-resident memory T cells

*Correspondence:
Zhijun Jie
jiezjlxh@163.com
Full list of author information is available at the end of the article

Background

Allergic asthma is characterized by chronic airway inflammation, bronchial hyperresponsiveness, reversible airflow limitation, and airway remodeling. Asthma leads to significant disability, reduced quality of life, and even death among children and young adults [1]. Impaired immune tolerance to particular antigens characterized by a hyperactive immune response has been reported in patients with allergic asthma [2]. Immune tolerance is a key pathogenic factor of allergic asthma [3–5]. Sublingual immunotherapy has been explored as a potential treatment strategy for asthma; however, current evidence, particularly in the United States, where it is only available for house dust mites, has not demonstrated substantial clinical benefits. Nevertheless, reconstruction of oral tolerance could be a potential treatment strategy [6, 7]. Different types of cells participate in maintaining immune tolerance, including plasmacytoid dendritic cells [8] and regulatory T cells mediated by Notch4 signaling [9].

Several reports have suggested that $CD4^+CD44^+$ memory T cells contribute to immune tolerance [10, 11]. $CD4^+CD44^+$ memory T cells could generally be divided into three subtypes: tissue-resident memory T (TRM) cells and two types of circulating memory T cells: effector memory T (TEM) and central memory T (TCM) cells [12, 13]. The homing molecules CD62L and CD69 aid in distinguishing each population (TEM: $CD62L^-CD69^-$, TCM: $CD62L^+CD69^-$, TRM: $CD62L^-CD69^+$) [14–16]. TRM cells constitute the most abundant subset of tissue memory T cells [17]. These cells can be generated in situ when exposed to pathogen and can persist in non-lymphoid tissues for an extended period, contributing to rapid and critical immune responses [18]. TRM cells constitute the frontline responders to chronic asthmatic inflammation in BALB/c and C57BL/6 mice [19–21]. Several transcription factors, including T-BET and EOMES, promote $CD4^+$ TRM cell development [22]. However, it remains unclear whether TRM cells interfere with immune tolerance. Additionally, the mechanisms underlying $CD4^+$ TRM cell development have not been fully elucidated.

In the present study, we investigated the role of $CD4^+$ TRM cells in immune tolerance using asthma and oral tolerance mouse models. The relationships between the proportion of $CD4^+$ TRM cells and asthma severity were evaluated. Moreover, $CD4^+$ T cells were isolated from the lungs and spleens of asthmatic model mice and transferred to oral tolerance mouse models. Conditional knockout studies identified promising therapeutic targets for asthma. Experiments in vitro and in vivo were performed to identify the key factors facilitating $CD4^+$ TRM cell differentiation. This research provides valuable insights into the immunological mechanisms of asthma and highlights potential therapeutic targets for improving immune tolerance in allergic diseases.

Methods

Animals

Female BABL/c and C57 (16–18 g) mice aged 3–4-weeks old were purchased from the Beijing Weitong Lihua Laboratory Animal Technology Co.,ltd. (Beijing, China) and housed at East China Normal University Animal Center. Zbtb16-flox mice (strain no. T016043) were purchased from GemPharmatech (Nanjing, China). CD4 Cre mice (strain no. 022071) were purchased from the Jackson Laboratory. The mice were housed in groups (4–6 mice/cage) at 21–24 °C with 12-h dark/light cycles and free access to food and water under specific pathogen-free conditions. The mice were randomly assigned to groups and allowed to acclimate substantially for 1 week before the experiments. Anesthesia was induced via an intraperitoneal (i.p.) injection of pentobarbital sodium (50 mg/kg) before the mice were euthanized.

Establishing the asthma and oral tolerance mouse model

BALB/c, C57 and $Zbtb16^{flox/flox}$ $CD4^{Cre}$ mice (3–4 weeks old) were randomly divided into three groups ($n=4–6$): (i) Control mice: administered placebo on day 0 and allowed to rest for 1 week before a single dose of alum (50 μL of alum gel in 70 μL of PBS) was administered i.p. on day 14 and PBS was aerosolized (40 min/d) on days 21–27; (ii) Asthma model: administered placebo on days 0–7, allowed to rest for 1 week before a single dose of ovalbumin (OVA)/alum (50 μg of OVA and 50 μL alum gel in 70 μL of PBS) was administered i.p. on day 14 and OVA was aerosolized (10 mg/mL in PBS, 40 min/d) on days 21–27 [23, 24]; and (iii) Oral tolerance (Oral tolerance, OT) model: fed OVA (1% dissolved in sterile water) on days 0–7 and allowed to rest for 1 week before a single dose of OVA/alum was administered i.p. on day 14 and OVA was aerosolized (50 μg of OVA and 50 μL alum gel in 70 μL of PBS). Mice were euthanized 24 h after the last aerosol challenge.

Hematoxylin and Eosin (H&E) staining

Lung sections were first deparaffinized in xylene and rehydrated through graded ethanol to distilled water. Hematoxylin was applied to stain nuclei, followed by differentiation in acid alcohol and bluing in alkaline water. Eosin was then used to counterstain cytoplasmic structures. Finally, the sections were dehydrated, cleared in xylene, and mounted with coverslips.

Periodic Acid-Schiff (PAS) staining

Periodic Acid-Schiff (PAS) staining was used to detect polysaccharides and mucosubstances. Tissue sections

were deparaffinized and rehydrated to distilled water, then oxidized with periodic acid to generate aldehyde groups. Schiff reagent was applied to react with the aldehydes, producing a magenta color. Hematoxylin was used as a counterstain for nuclei, and the sections were subsequently dehydrated, cleared, and mounted.

Masson's Trichrome staining

Masson's Trichrome staining was conducted to differentiate collagen fibers from other tissue components. After deparaffinization and rehydration, nuclei were stained with Weigert's hematoxylin. Acid fuchsin was used to stain cytoplasm and muscle fibers, followed by differentiation with phosphomolybdic acid. Collagen fibers were stained with aniline blue or light green. The sections were then dehydrated, cleared, and mounted for microscopic examination.

Asthma-Mem and OT-Mem mouse models

The modeling process was identical to that described for the first 27 days (without aerosol challenge) for the control, asthma, and OT mouse models. The mice were allowed to recover for at least 5 weeks and were euthanized every 7 days (asthma-mem and OT-mem mouse models). Subsequently, relapse was induced via a single intranasal (i.n.) OVA challenge (100 μg) in 50 μL of PBS with light anesthesia on days 69 and 70. The mice were analyzed for cell populations on days 71, 78, and 85.

FTY720 model

Asthma mice were allowed to rest until days 66–73 and then injected i.p. with FTY720 (2.0 μg/g bodyweight; SelleckChem, Houston, TX, USA) dissolved in sterile water ($n=4$–6/group) [25, 26]. On days 69–70, FTY720 was injected i.p. 2 h before single i.n. OVA challenges (100 μg) in 50 μL of PBS.

Real-time qPCR

Total RNA was extracted from the lungs using an AFT-Spin Tissue/Cell Fast RNA Extraction Kit for Animals (ABclonal, Wuhan, China) following the manufacturer's instructions. The RNA concentration was determined using a NanoDrop 2000 spectrophotometer (Thermo Fisher Scientific, Waltham, MA, USA). cDNA was synthesized with ABScript III RT Master Mix for quantitative polymerase chain reaction (qPCR) with a gDNA Remover kit (ABclonal, Wuhan, China) and subjected to RT–qPCR analysis with Taq Pro Universal SYBR qPCR Master Mix (Vazyme, Q712-02) (Tables 1 and 2).

Western blotting

A total of 30 mg of mouse lung tissue was finely minced and 150 μL of RIPA lysis buffer containing protease inhibitor was added. The suspension was ground thoroughly with a tissue grinder. After centrifugation at 12,000×*g* for 5 min, the total protein in the supernatant

Table 2 Reaction conditions for qPCR

Stage 1	Initial denaturation	Rep:1	95℃	30 s
Stage 2	Cycling reaction	Reps:40	95℃	3—10 s
			60℃	10—30 s
Stage 3	Melting curve analysis	Rep:1	95℃	15 s
			60℃	60 s
			95℃	15 s

Table 1 Primers used in qPCR

Gene name	Forward sequence	Reverse sequence
Il4	ATCATCGGCATTTTGAACGAGGTC	ACCTTGGAAGCCCTACAGACGA
Il5	GATGAGGCTTCCTGTCCCTACT	ACCTTGGAAGCCCTACAGACGA
Gapdh	CATCACTGCCACCCAGAAGACTG	TGACAGGTTTTGGAATAGCATTTCC
Il13	AAAGCAACTGTTTCGCCACG	CCTCTCCCCAGCAAAGTCTG
Zbtb16	CTGGGACTTTGTGCGATGTG	CGGTGGAAGAGGATCTCAAACA
Il15rb	CTCAAGTGCCACATCCCAGATC	AGCACTTCCAGCGGAGAGATCT
Il15ra	GACACCAAAGGTGACCTCACAG	CTGTCTCTGTGGTCATTGCGGT
Il15	GTAGGTCTCCCTAAAACAGAGGC	TCCAGGAGAAAGCAGTTCATTGC
Il7	CAGGAACTGATAGTAATTGCCCG	CTTCAACTTGCGAGCAGCACGA
Il7r	CACAGCCAGTTGGAAGTGGATG	GGCATTTCACTCGTAAAAGAGCC
Dll4	GGGTCCAGTTATGCCTGCGAAT	TTCGGCTTGGACCTCTGTTCAG
Jagged2	CGCTGCTATGACCTGGTCAATG	TGTAGGCGTCACACTGGAACTC
Zbtb16$^{flox/flox}$	TTGGGCCTTAGAGATGAGGAGAAAG	CCCTCATTGCTTTAACACTGGTACTC
Cd4^{cre}	CCTGATCCTGGCAATTTCGG	CCCAACCAACAAGAGCTC

was retrieved. The protein concentration was determined using the Pierce BCA protein assay kit (Thermo Fisher Scientific). Next, 60 μg protein samples were separated via 12% SDS-PAGE and transferred onto polyvinylidene difluoride (PVDF) membranes (Millipore, Bedford, MA, USA). After blocking, the membranes were incubated with appropriate primary antibodies at 4 °C overnight: CD215/interleukin (IL)−15R alpha rabbit pAb (NO. A2983, 1:500; ABclonal, Wuhan, China), IL-2RB rabbit pAb (NO. A6207, 1:100; ABclonal), CD127/IL-7R rabbit mAb (NO. A11678, 1:1000; ABclonal), DLL4 rabbit pAb (NO. A12943, 1:1000; ABclonal), JAG2 rabbit pAb (NO. A1424, 1:500; ABclonal), Hsp90α rabbit pAb (NO. A12448, 1:1000; ABclonal), JAK1 rabbit mAb (NO.3344, 1:1000, Cell signaling Technology, Danvers, USA) and JAK3 mAb (NO.8827, 1:1000, Cell signaling Technology). After washing with TBST, the membranes were incubated with an anti-rabbit IgG HRP-conjugated antibody (Cell Signaling Technology, NO. 7074, 1:5000), and the protein bands were visualized via chemiluminescence (Thermo Fisher Scientific) using a Tanon 5200 imaging system (Biotanon, Shanghai, China). The protein expression levels were quantified using ImageJ v1.48 software (National Institutes of Health (NIH), Bethesda, MD, USA).

Single-cell suspensions

Mice were injected intravascularly with 3 mg APC/Cyanine7 anti-mouse CD45 (BioLegend, California, USA) in 300 μL of Dulbecco's phosphate-buffered saline (DPBS) [27, 28]. After 10–15 min, the mice were euthanized. The lungs and spleen were digested separately with 50 μg/mL Liberase (Roche, Basel, Switzerland) and 1 μg/mL DNase I at 37 °C for 50 min with shaking (200 rpm). The digested tissue was centrifuged at 500×*g* for 7 min at 4 °C. Cells were collected after lysing erythrocytes for 7 min (lung tissue) or 10 min (spleen tissue) using Red Blood Cell Lysis Buffer (Beyotime, Shanghai, China). Finally, single-cell suspensions were obtained with a 70 μM (lung tissue) or 40 μM (spleen tissue) cell strainer (BD Biosciences, New Jersey, USA).

Flow cytometry

The cell suspensions were incubated with purified rat anti-mouse CD16/CD32 (Clone 2.4G2; BD Biosciences) to block Fc fragments on immune cells for 15 min at 4 °C. Before surface staining, the cells were stained with a Zombie UV™ Fixable Viability Kit (BioLegend) in PBS (1:100) for 20–30 min at room temperature in the dark to distinguish live cells. Next, monoclonal antibodies specific for surface markers were added to the cells and incubated for 30 min at 4 °C in the dark: Brilliant Violet 510™ anti-mouse CD3ε (17A2), FITC anti-mouse CD4 antibody (RM4-5), PerCP/Cyanine5.5 anti-mouse/human CD44 (IM7), APC anti-mouse CD62L (MEL-14), Brilliant Violet 605™ anti-mouse CD62L (MEL-14), PE/Cyanine7 anti-mouse CD69 (H1.2F3), APC anti-mouse CD215 (IL-15Rα) (6B4C88) and Compensation Beads (all from BioLegend).

A Transcription factor buffer set (BD Biosciences) was used for intranuclear staining. Nuclear membranes were fixed and permeabilized with 1×Fix/Perm Buffer for 40–50 min at 4 °C. A PE anti-mouse PLZF antibody (9E12) was suspended with cells in 100 μL of 1×Perm/Wash buffer at 2–8 °C for 40–50 min in the dark (BioLegend).

A Cytofix/Cytoperm with GolgiPlug kit (BD Biosciences) was used for intracellular staining. The cells were incubated in 6-well plates in a humidified atmosphere containing 5% CO_2 at 37 °C for 6 h with 50 ng/mL phorbol 12-myristate 13-acetate (PMA) and 1 μg/mL ionomycin (to stimulate cytokine production), and 1 μg/mL GolgiPlug™ protein transport inhibitor. Next, the cells were suspended with fixation/permeabilization solution for 20 min at 4 °C. These cells were incubated with 50 μL of BD Perm/Wash buffer containing the following fluorochrome-conjugated antibodies at 4 °C for 30 min in the dark: Brilliant Violet 421™ anti-mouse IL-4 (11B11), APC anti-mouse/human IL-5 (TRFK5) and PE anti-mouse IL-13(W17010B) (all from BioLegend).

All samples were filtered through a 40-μM strainer prior to flow cytometry. Data were acquired with an LSR-Fortessa™ flow cytometer (BD Biosciences) and Beckman Coulter CytoFlex (Beckman Coulter, USA). All data were analyzed with FlowJo software (TreeStar, Ashland, OR, USA) and CytExpert (Beckman Coulter)..

Lung immunofluorescence and microscopy

Mice were euthanized, and their entire lungs were removed and fixed in 4% paraformaldehyde. The tissues were embedded in paraffin or optimal cutting temperature (OCT) compound for cryosectioning. For paraffin-embedded tissues, a microtome was used 5 μm sections. Single-label immunofluorescence staining of CD4 in the lung tissues was performed with an anti-CD4 mouse monoclonal antibody (Abcam). The fluorescent Cy3-conjugated goat anti-mouse IgG secondary antibody (Powerful Biology, Wuhan, China) was then added. Dual-label immunofluorescence staining of CD4 and IL15Rα in the lung tissues was performed with anti-CD4 and anti-IL15Rα mouse monoclonal antibody (Abcam). The fluorescent Cy3-conjugated and Cy5 goat anti-mouse IgG secondary antibody (Powerful Biology, Wuhan, China) was then added. Additionally, 4′,6-diamidino-2-phenylindole (DAPI; Powerful Biology) was used to stain the nuclei. Images were acquired with an Olympus FV1200

laser scanning microscope and analyzed by CaseVeiwer 7.2.

Collection of plasma and IgE levels detection

Mice were anesthetized, and approximately 0.5–1.0 mL of cardiac blood was collected in tubes containing ethylenediaminetetraacetic acid (EDTA) to prevent coagulation. After centrifugation at 1500×*g* for 10 min at 4 °C, the upper layer (plasma) was transferred into a 1.5 mL tube and stored at − 80 °C. The levels of total IgE in serum samples were quantified using the BD OptEIA™ Mouse IgE ELISA Kit (BD Biosciences, USA) following the manufacturer's protocol. Briefly, 96-well microplates pre-coated with anti-human IgE monoclonal antibodies were used. Standards, controls, and diluted serum samples (100 µL per well) were added to the plate and incubated at room temperature for 2 h. After washing the plate five times with the provided wash buffer, 100 µL of biotinylated anti-IgE detection antibody was added to each well and incubated for 1 h at room temperature. Following another washing step, 100 µL of streptavidin–horseradish peroxidase (HRP) conjugate was added and incubated for 30 min at room temperature. After a final wash, 100 µL of tetramethylbenzidine (TMB) substrate solution was added to each well and incubated in the dark for 15 min. The reaction was stopped by adding 50 µL of stop solution (1 M H_2SO_4), and the optical density (OD) was measured at 450 nm using a microplate reader (Nanoquant 2000pro, Zurich, Switzerland).

Collection of bronchoalveolar lavage fluid (bronchoalveolar lavage fluid, BALF)

BALF was collected via a tracheal incision and washing the lungs thrice with 1 mL of PBS each time. The BALF was centrifuged at 500×*g* for 15 min at 4 ℃, and BALF cells were collected from the pellet. The supernatant was stored at − 80 ℃ until eosinophilic granulocyte observation and IL-15 detection.

IL15 levels detection

The levels of mouse IL-15 in the samples were quantified using the Mouse IL-15 ELISA Kit (Catalog No.: RK00106, ABclonal, China) following the manufacturer's instructions. The assay was based on a sandwich ELISA principle. Briefly, 96-well microplates pre-coated with anti-IL-15 antibodies were used. Standards and samples (100 µL per well) were added to the wells, incubated at 37 °C for 2 h, and washed thrice with 350 µL of 1×Wash Buffer to remove unbound components. Next, 100 µL of biotin-conjugated anti-IL-15 antibody, prepared by diluting the concentrated antibody (100×) in Biotin-Conjugate Antibody Diluent (R2), was added to each well. The plate was sealed and incubated at 37 °C for 1 h. After washing the wells thrice, 100 µL of streptavidin-HRP working solution, prepared by diluting the concentrated streptavidin-HRP (100×) in Streptavidin-HRP Diluent (R3), was added to each well. The plate was incubated at 37 °C for 30 min. Following another washing step, 100 µL of TMB substrate solution was added to each well and incubated at 37 °C in the dark for 15–20 min. The reaction was stopped by adding 50 µL of Stop Solution to each well. The OD was measured at 450 nm using a microplate reader, with a reference wavelength of 570 nm or 630 nm to correct for background absorbance.

Lymphocytes purification and magnetic bead cell sorting (CD4 $^+$T cells)

A lung cell suspension was acquired in 3.9 mL of Roswell Park Memorial Institute (RPMI)−1640. Next, 1.215 g/mL OptiPrep™ Working Solutions (four volumes OptiPrep™ (60%, w/v iodixanol) in two volumes of RPMI-1640) was added and gently mixed. Subsequently, 1 mL of RPMI-1640 was added to cover the liquid and centrifuged at 1500×*g* for 20 min at 4 °C. Lymphocytes were collected and resuspended in up to 4 mL of MojoSort™ Buffer in a 5 mL polypropylene tube. The cells were filtered with a 70 µM cell strainer, centrifuged at 300×*g* for 5 min, and resuspended in an appropriate volume of MojoSort™ Buffer. Aliquots (100 µL) containing a 1×10^6 cell suspension were placed into a new tube, and 10 µL of the Biotin-Antibody Cocktail was added and incubated for 15 min on ice. The beads were resuspended by vortexing at maximum speed. A volume of 10 µL of the Streptavidin Nanobeads was added to each tube, mixed well, and incubated on ice for 15 min. Next, 2.5 mL of MojoSort™ Buffer was added, and the tube was placed on a magnet for 5 min to isolate $CD4^+$ T cells, which were subsequently collected.

$CD4^+$ T Cell Isolation and CUT&Tag Assay

$CD4^+$ T cells were isolated from mouse spleen or lymph nodes using fluorescence-activated cell sorting (FACS). Single-cell suspension preparation has been described above. Cells were stained with fluorochrome-conjugated anti-CD4 antibodies (BioLegend) and sorted using a BD FACSAria III flow cytometer (BD Biosciences). The purity of the sorted $CD4^+$ T cells was assessed by re-analysis on the flow cytometer and was consistently > 90%.

The CUT&Tag assay was performed to investigate the genome-wide binding profile of PLZF in $CD4^+$T cells using the Hyperactive In-Situ ChIP Library Prep Kit for Illumina (Vazyme, China) with modifications based on the protocol. Approximately 100,000 FACS-sorted $CD4^+$ T cells were washed twice with ice-cold PBS and resuspended in Wash Buffer (20 mM HEPES, pH 7.5, 150 mM NaCl, 0.5 mM spermidine, and 1×Protease Inhibitor Cocktail). Cells were bound to Concanavalin A-coated

magnetic beads (Bangs Laboratories, Indiana, USA) following the manufacturer's instructions. The bead-bound cells were incubated with 10 μL of PLZF antibody (Affinity Biosciences, Catalog No.: DF7517, 1:50 dilution) in Antibody Buffer (Wash Buffer supplemented with 2 mM EDTA and 0.05% digitonin) at 4 °C overnight with gentle rotation. A rabbit IgG isotype control (Cell Signaling Technology) was included as a negative control. After washing with Wash Buffer containing 0.05% digitonin, cells were incubated with 1:100 diluted secondary antibody (anti-rabbit IgG conjugated to pA-Tn5 transposase, Vazyme) in Antibody Buffer at room temperature for 1 h with gentle rotation. Following secondary antibody binding, cells were washed and resuspended in Tagmentation Buffer (10 mM MgCl2 in Wash Buffer with 0.05% digitonin) and incubated at 37 °C for 1 h to facilitate tagmentation of chromatin at PLZF binding sites. The reaction was stopped by adding Stop Buffer (Vazyme), and DNA was extracted using a DNA purification kit (Qiagen, Germany).

Extracted DNA was amplified by PCR using indexed primers provided in the Hyperactive In-Situ ChIP Library Prep Kit. The amplified libraries were purified using AMPure XP beads (Beckman Coulter) and quantified using a Qubit Fluorometer (Thermo Fisher Scientific). Library quality was assessed using an Agilent 2100 Bioanalyzer, and sequencing was performed on an Illumina NovaSeq 6000 platform to generate paired-end 150 bp reads.

Isolation and culture of lymphocytes from the lungs and spleen

BEAS-2B cells, a human bronchial epithelial cell line, were cultured in DMEM/F12 medium (Gibco, Massachusetts, USA) supplemented with 10% fetal bovine serum (FBS, Gibco) and 1% penicillin–streptomycin (Gibco) at 37 °C in a humidified atmosphere containing 5% CO_2. Once the cells reached approximately 70–80% confluence, they were washed twice with sterile PBS. For in vitro stimulation, the cells were treated with 100 μg/mL OVA (Grade V, Sigma-Aldrich, Missouri, USA) diluted in serum-free DMEM/F12 medium and incubated for 36 h under standard culture conditions (37 °C, 5% CO_2). Control cells were treated with serum-free DMEM/F12 medium without OVA under the same conditions. After 36 h of stimulation, the cell culture supernatants were collected by aspirating the medium to avoid disturbing the cell monolayer, followed by centrifugation at 1000 × *g* for 10 min at 4 °C to remove cell debris. The supernatants were aliquoted into sterile tubes and stored at − 80 °C until further analysis, with aliquots prepared in volumes suitable for single-use experiments to avoid repeated freeze–thaw cycles.

Wild-type and Zbtb16-cKO C57BL/6 mice (6–8 weeks old) were euthanized. The spleens were removed from each mouse, ground gently, and passed through a 70 μM cell strainer with 5–6 mL Mouse Lymphocyte Separation Medium (Dakewe™) into a 15 mL centrifuge tube. Density gradient separation of spleen lymphocytes was then performed.

Lungs were removed and single-cell suspensions were prepared as described above. The lymphocytes were counted with a hemocytometer and cultured in RPMI-1640 containing 10% (vol/vol) FBS for 24 h. Lymphocytes were stimulated with the supernatant from 36-h OVA-treated BEAS-2B cell cultures and 15 ng/mL recombinant mouse IL-15 (No.566302, BioLegend) for 24 h (Fig. 8f). Thereafter, cells were collected and analyzed via flow cytometry.

Statistical analysis

All data were analyzed using Prism 8.0 software (GraphPad Software, CA, USA). Data were expressed as mean ± standard error of the mean (SEM). Differences between two groups were analyzed using an unpaired two-tailed Student's t test. Differences among more than three groups were analyzed using one way ANOVA test. Results were considered statistically significant at $P < 0.05$.

Results

$CD4^+CD44^+$ memory T cells are enriched in the lungs of murine asthma models

We first established the pathological (asthma) and OT models (Fig. 1a). OVA was used as an allergen to stimulate the immune response and to establish oral tolerance, mice were also fed 1% OVA in the OT group prior to primary immunization (Fig. 1a). Classic allergic asthma phenotypes, including inflammatory cell infiltration, mucus hypersecretion, and smooth muscle contraction, were observed in the airways of the asthma group after OVA inhalation for 7 days (Fig. 1b, c) [29]. More specifically, the Periodic acid–Schiff (PAS) staining of lung tissues from asthmatic mice showed increased goblet cell hyperplasia and mucus production in the airway epithelium. Masson's trichrome staining revealed enhanced collagen deposition and airway remodeling, indicating fibrosis in the lung tissue (Fig. S1a, b). Meanwhile, no obvious histopathological changes were observed in the OT group compared with the control group (Fig. 1b).

Furthermore, we evaluated the expression of genes encoding type 2 (T2) cytokines, including *Il4, Il5,* and *Il13*, as well as the secreted IgE levels, as indicators of the allergic response [30]. Significant increases were detected in each of these markers in the asthma group but not in the control or OT groups (Fig. 1d, e). Collectively,

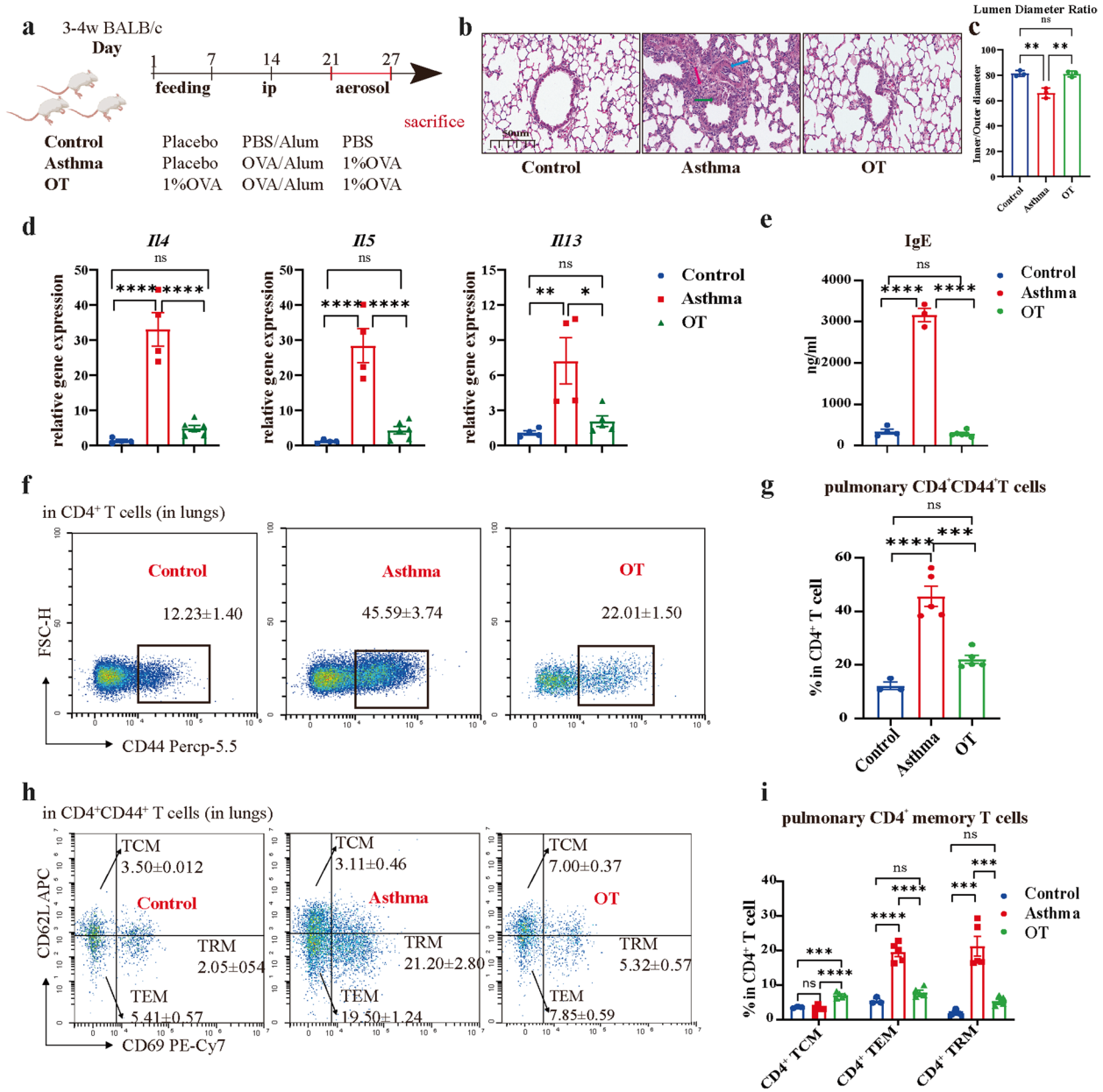

Fig. 1 CD4$^+$CD44$^+$T cells, particularly CD4$^+$TEM cells and CD4$^+$ TRM cells, are abundant in asthma mouse models. **a** Successful establishment of asthma and oral tolerance (OT) models ($n = 4–6$). **b** Representative microphotographs of lung histological sections from control, asthmatic, and OT mice in objective magnification × 29. Green arrow: swollen airway; Red arrow: inflammatory cell infiltration; Blue arrow: congestive small blood vessels. **c** Ratio of the inner diameter to the outer diameter, evaluating airway smooth muscle contraction. **d** mRNA expression of *Il4, Il5,* and *Il13* in the whole lung tissues assessed by real-time qPCR. **e** Plasma IgE levels assessed by ELISA. **f**, **g** Proportion of pulmonary CD4$^+$CD44$^+$ cells in CD4$^+$ T cells detected by flow cytometry. **h**, **i** Flow cytometric analysis of CD4$^+$ TCM, CD4$^+$ TEM, and CD4$^+$ TRM cells in lungs of control, asthma, and OT model mice. All bars indicate mean ± SEM. Data in **c**, **d**, **e, g**, **i** were analyzed using one-way ANOVA. *$P < 0.05$, **$P < 0.01$, ***$P < 0.001$, ****$P < 0.0001$, ns: not significant. TCM: central memory T cells, TEM: effector memory T cells, TRM: resident memory T cells

these results confirm the successful creation of allergic asthma and an OT model with histological and molecular characteristics.

To explore the relationship between CD4$^+$CD44$^+$ memory T cells and allergic asthma, we performed flow cytometry with the three models. Compared with mice in the control or OT groups, CD4$^+$CD44$^+$ memory T cells were significantly enriched in the lungs of the asthma group, whereas relatively subtle changes occurred in the control and OT groups (Fig. 1f, g). In particular, CD4$^+$

TRM and $CD4^+$ TEM cells may have been responsible for the high proportion of $CD4^+CD44^+$ memory T cells in the asthma group (Fig. 1h, i). Comparable differences were not observed in the spleens of model animals. Considering that the spleen serves as the germinal zone of circulating memory T cells, the results suggest a specific immune response in the lungs of the asthma group (Fig. S1c–f). We hypothesized that elevated $CD4^+CD44^+$ memory T cells, particularly $CD4^+$ TRM and $CD4^+$ TEM cells, contribute to impaired immune tolerance and asthma pathogenesis.

Changes in $CD4^+CD44^+$ memory T cells positively correlate with asthma symptoms

To characterize the temporal pattern of the immune responses in our models, mice were euthanized at different time points over a 5-week period (days 28 to 63) of rest after inducing allergic airway inflammation and relapse with 0.2% OVA on days 69 and 70 (Fig. 2a). This duration is sufficient to generate circulating memory cells [21]. Attenuated allergic phenotypes, as well as decreased IgE secretion, were observed in the asthma-mem group over time (Fig. 2b). Histological analysis indicated that the lungs of the asthma-mem group exhibited a more advanced pathological state than those of the control-mem or OT-mem groups (Fig. 2c and Fig. S2a). However, significant differences were not observed in secreted IgE levels between the groups after resting for 5 weeks (Fig. 2b). A similar decreasing trend in $CD4^+CD44^+$ T cells was observed in the lungs of the asthma-mem group (Fig. 2d). The proportion of $CD4^+CD44^+$ T cells remained relatively stable over the first 3 weeks and tended to decrease during the following 2 weeks.

We also performed restimulation by intranasal delivery of low OVA concentration (i.e., Mem group). Changes in the $CD4^+CD44^+$ T cell proportion correlated with the pathological state (Fig. 2c, d). Asthma-Mem (day 71) mice exhibited allergic phenotypes, including an inflamed airway and inflammatory cell proliferation, for at least 2 weeks (Fig. 2c and Fig. S2a). A markedly greater increase in T2 cytokine expression was also detected, whereas secreted IgE levels did not differ significantly between the Mem groups (Fig. S2b). Thus, mucosal $CD4^+$ memory cells may have become activated more rapidly than the delayed B-cell-related immune responses during restimulation with the same antigen. In addition to severe allergic phenotypes, the proportion of $CD4^+CD44^+$ memory T cells also increased (Fig. 2d). Taken together, these findings suggest that the

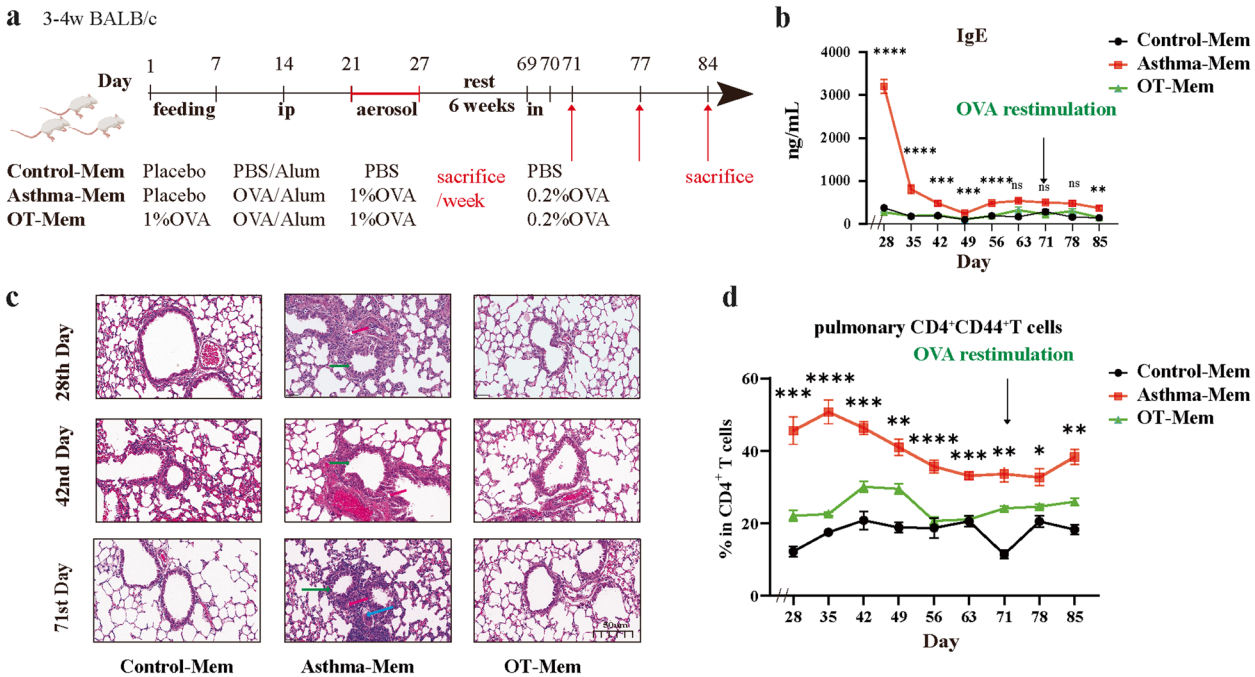

Fig. 2 $CD4^+CD44^+$ T cell proportion is persistently increased in the Asthma-mem group and upon asthma relapse. **a** Scheme of Control-mem, Asthma-mem, and oral tolerance (OT)-mem models ($n = 4$–6/group). **b** Plasma IgE levels assessed by ELISA over 56 days. **c** Representative microphotographs of lung histological sections from Control-mem, Asthma-mem, and OT-mem mice in objective magnification × 29 on days 28, 42, and 71. Green arrow: inflamed airway; Red arrow: inflammatory cell infiltration; Blue arrow: congestive small blood vessels. **d** Flow cytometric detection of proportion of pulmonary $CD4^+CD44^+$ cells. All bars indicate mean ± SEM. Data in **b, d** were analyzed using unpaired two-tailed Student's *t*-test. $^*P < 0.05$, $^{**}P < 0.01$, $^{***}P < 0.001$, $^{****}P < 0.0001$, ns: not significant

proportion of $CD4^+CD44^+$ memory T cells in the lung is strongly positively correlated with allergic symptoms in mice with asthma.

$CD45^-CD4^+$ TRM cells dominate changes in $CD4^+CD44^+$ memory T cells and T2 cytokines, inducing the relapse of asthma-related Th2 inflammation

Considering that $CD4^+CD44^+$ memory T cells can be categorized according to CD62L and CD69 expression, we sought to identify the subtype responsible for the observed differences in $CD4^+CD44^+$ memory T cell proportion. Immediately after inducing the allergic response, there was a notable increase in the proportions of $CD4^+$ TEM and $CD4^+$ TRM cells in the asthma group than in the other groups (Fig. 1g, h). Similar results were observed in the restimulation experiments (Fig. S2c). However, the temporal pattern of these two subtypes was unusual, potentially due to insufficient definition of cell types and limited use of cell surface markers (Fig. 3a, b). Thus, to precisely define the cell composition, we administered the fluorescent antibody APC-Cy7 CD45 to mice via intravascular injection to discriminate vascular and tissue memory T cells (Fig. 3c). Indeed, CD45 is a critical cell surface marker expressed by leukocytes; intravascular staining can effectively distinguish between tissue-localized and blood-borne cells in non-lymphoid tissues [27]. Significant enrichment of $CD45^-CD4^+$ TRM cells, not $CD45^+CD4^+$ TEM cells, was observed in the lungs of the asthma and asthma-mem groups, suggesting enrichment of tissue-localized cells. Similarly, the proportion of $CD45^-CD4^+$ TRM cells decreased compared with $CD4^+CD44^+$ memory T cells during the remaining study period. In contrast, the proportion of $CD45^+CD4^+$ TEM cells did not differ among groups (Fig. 3d, e). These results suggested that $CD4^+$TRM cells were responsible for the increased $CD4^+CD44^+$ memory T cell proportion during asthma pathogenesis. Functionally, a substantially greater proportion of TRM cells produced IL-4, IL-5 and IL-13 than other memory T cell subtypes. Hence, the increase in T2 cytokine levels may be directly related to the increased TRM cell proportion (Fig. 3f–h).

To further validate the importance of $CD4^+$ TRM cells, we inhibited peripheral lymphatic circulation by administering FTY720 to facilitate the collection of relatively pure TRM cells from tissues [31, 32] (Fig. 4a). Following FTY720 treatment, various T cell subsets decreased significantly in the lungs, excluding $CD45^-CD4^+$ TRM cells, consistent with the effect of FTY720 (Fig. 4c–f). Meanwhile, after blocking the peripheral lymphatic circulation, asthma phenotypes were not ameliorated, and the IgE level was not affected (Fig. 4b, g). Although T2 cytokine levels decreased moderately, they remained significantly higher in the FTY270 group than in the control group (Fig. 4h). These findings reinforce the significance of TRM cells, likely serving as key factors in the substantial alterations observed in the memory T cell ratio and T2 cytokine levels.

Adoptive transfer of TRM cells impairs immune tolerance in the OT group

To determine whether $CD4^+$TRM cells are responsible for the disruption of immune tolerance in asthma, we purified $CD4^+$ T cells from the lungs and spleens of the asthma-mem-FTY720 model and transferred 10^6 cells intranasally to the OT model after inducing oral tolerance (Fig. 5a**,** Fig. S3, S4) [25, 33, 34]. Approximately 35% $CD4^+$ TRM cells in $CD4^+$ T cells were sorted in the lungs, and 35% $CD4^+$ TEM cells in $CD4^+$ T cells in the spleens. Histological analysis revealed increased immune cell infiltration within the inflamed airway of Lung Transfer OT (OLT) model mice (Fig. 5b), consistent with asthma phenotypes. These effects were more severe in the OLT group compared with the Spleen Transfer OT (OST) and OT groups. Obviously, $CD45^-CD4^+$ TRM cells increased in the transfer-OT group (Fig. 5c, d). A moderate but significant increase in the expression of T2 cytokines, including *Il4*, *Il5,* and *Il13*, was observed in the OLT group compared with the OT and OST groups (Fig. 5e). However, the IgE levels were not affected (Fig. 5f). This was likely due to the lack of abdominal sensitization and the transfer of insufficient TRM cells. Collectively, the adoptive transfer results

(See figure on next page.)

Fig. 3 $CD45^-CD4^+$ TRM cells dominate the increased proportion of $CD4^+CD44^+$ T cells with increased Type 2 (T2) cytokine secretion. **a**, **b** Dynamic curve of the proportion of pulmonary $CD4^+$ TRM and $CD4^+$ TEM cells in total $CD4^+$ T cells; Green arrow: time of OVA restimulation. **c** Intravascular injection flow antibody CD45 was used to distinguish the resident and circulating cells. **d** Flow cytometry analysis of $CD45^+CD4^+$ TEM and $CD45^-CD4^+$ TRM cells in lungs of Control-mem, Asthma-mem, and oral tolerance (OT)-mem mice. **f**, **g** T2 cytokine (IL-4, IL-5, and IL-13) secretion of $CD4^+$ TRM cells estimated by flow cytometry. **h** Comparison of IL-4, IL-5, and IL-13 secretion in pulmonary $CD4^+$ TCM, $CD4^+$ TEM, and $CD4^+$ TRM cells; bars indicate mean ± SEM. Data in **a**, **b**, **d**, **e** were analyzed using unpaired two-tailed Student's *t*-test and data in **f**, **g**, **h** were analyzed using one-way ANOVA. *$P < 0.05$, **$P < 0.01$, ***$P < 0.001$, ****$P < 0.0001$, ns: not significant, TEM: effector memory T cells, TRM: resident memory T cells, Mem: Memory

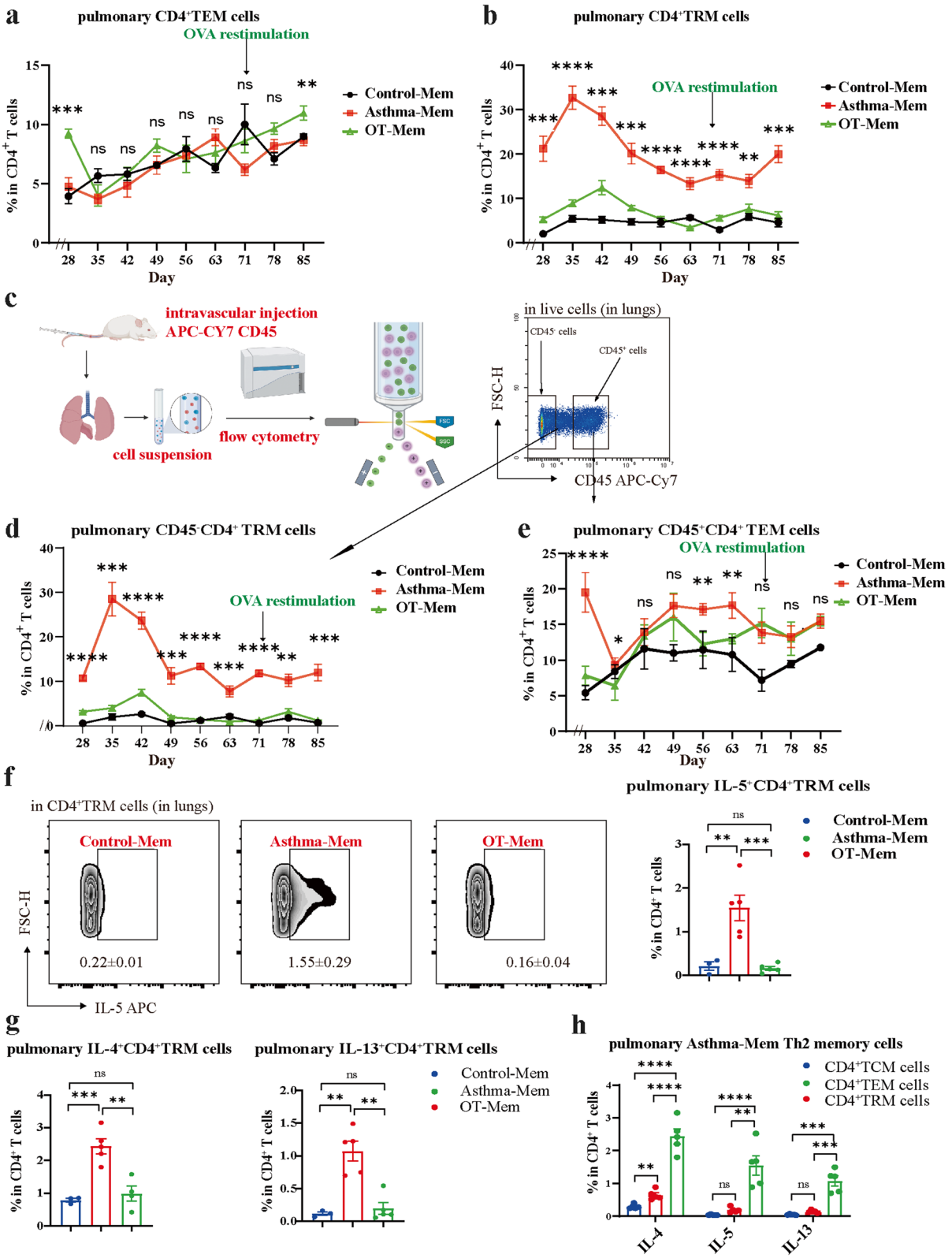

Fig. 3 (See legend on previous page.)

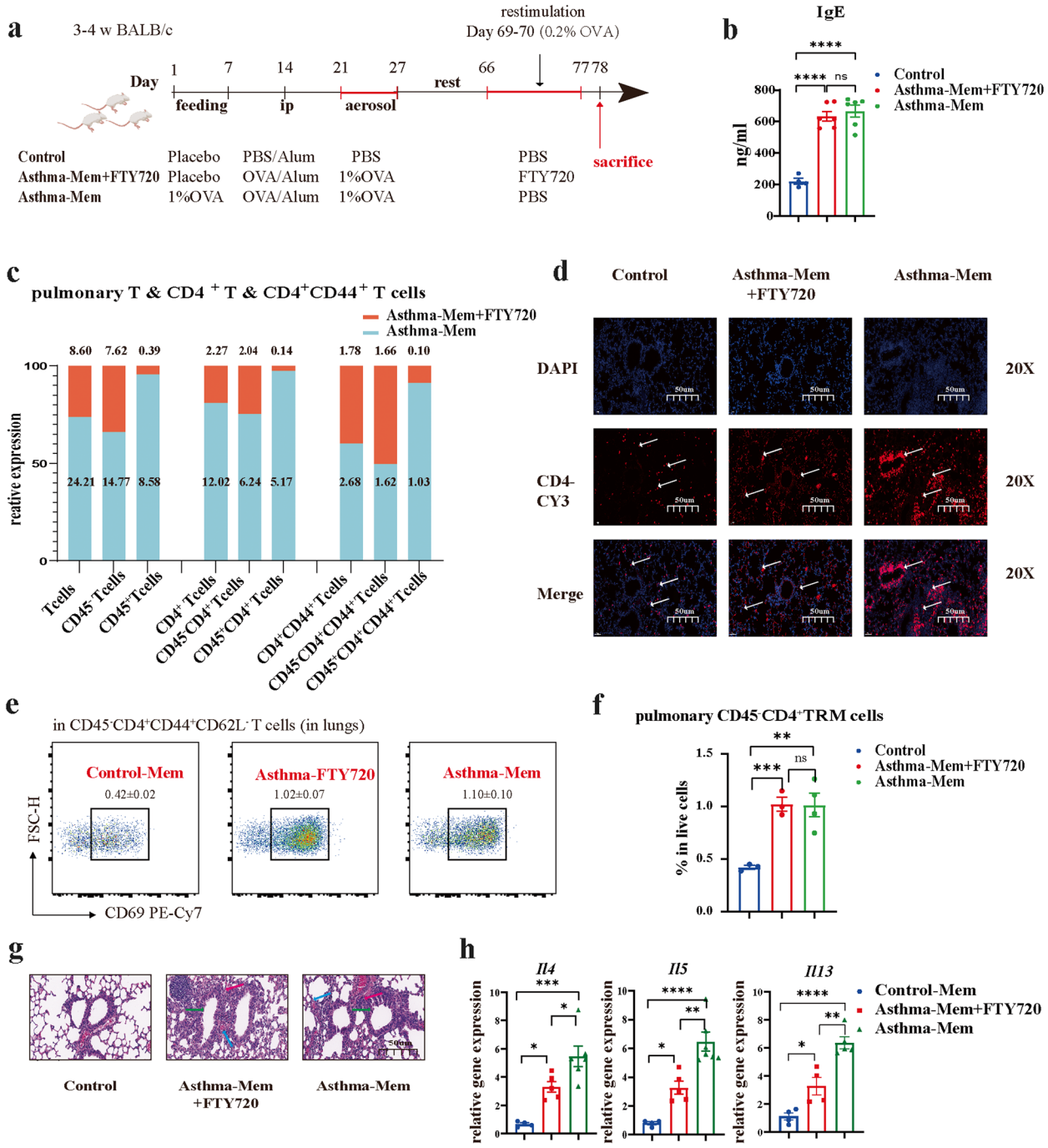

Fig. 4 CD4$^+$TRM cells can induce allergic inflammation in the early period. **a** Scheme of FTY720 treatment in asthma model mice ($n = 4–6$/group). FTY720 was injected into mice from day 67 to day 73, with 0.2% OVA relapse on days 69–70. **b** Comparison of plasma IgE levels assessed by ELISA. **c** Flow cytometric analysis of the relative proportion of pulmonary T cells, CD4$^+$ T cells, CD4$^+$CD44$^+$ T cells, and CD45$^-$ and CD45$^+$ T cells in Asthma-mem mice and FTY720-treated Asthma-mem mice. The proportion of each subset within the total cell population is presented above and on the columns. **d** Representative confocal images of lungs from Control-mem, Asthma-mem mice, and FTY720-treated Asthma-mem mice with single-labeled CD4-Cy3 (red) and DAPI (blue) in × 20 objective magnification; Scale bar, 50 μm; Arrows: CD4$^+$ T cells. **e**, **f** Comparison of the proportion of CD45$^-$CD4$^+$ TRM cells in the lungs. **g** Representative microphotographs of lung histological sections from Control-mem, Asthma-mem mice, and FTY720-treated Asthma-mem mice in × 29 objective magnification; Green arrow: inflamed airway; Red arrow: inflammatory cell infiltration; Blue arrow: congestive small blood vessels. **h** mRNA expression of *Il4, Il5,* and *Il13* in the whole lung tissues assessed by real-time qPCR. All bars indicate mean ± SEM. Data in **b**, **f**, **h** were analyzed using one-way ANOVA. *$P < 0.05$, **$P < 0.01$, ***$P < 0.001$, ****$P < 0.0001$, ns: not significant. TRM: resident memory T cells, Mem: Memory

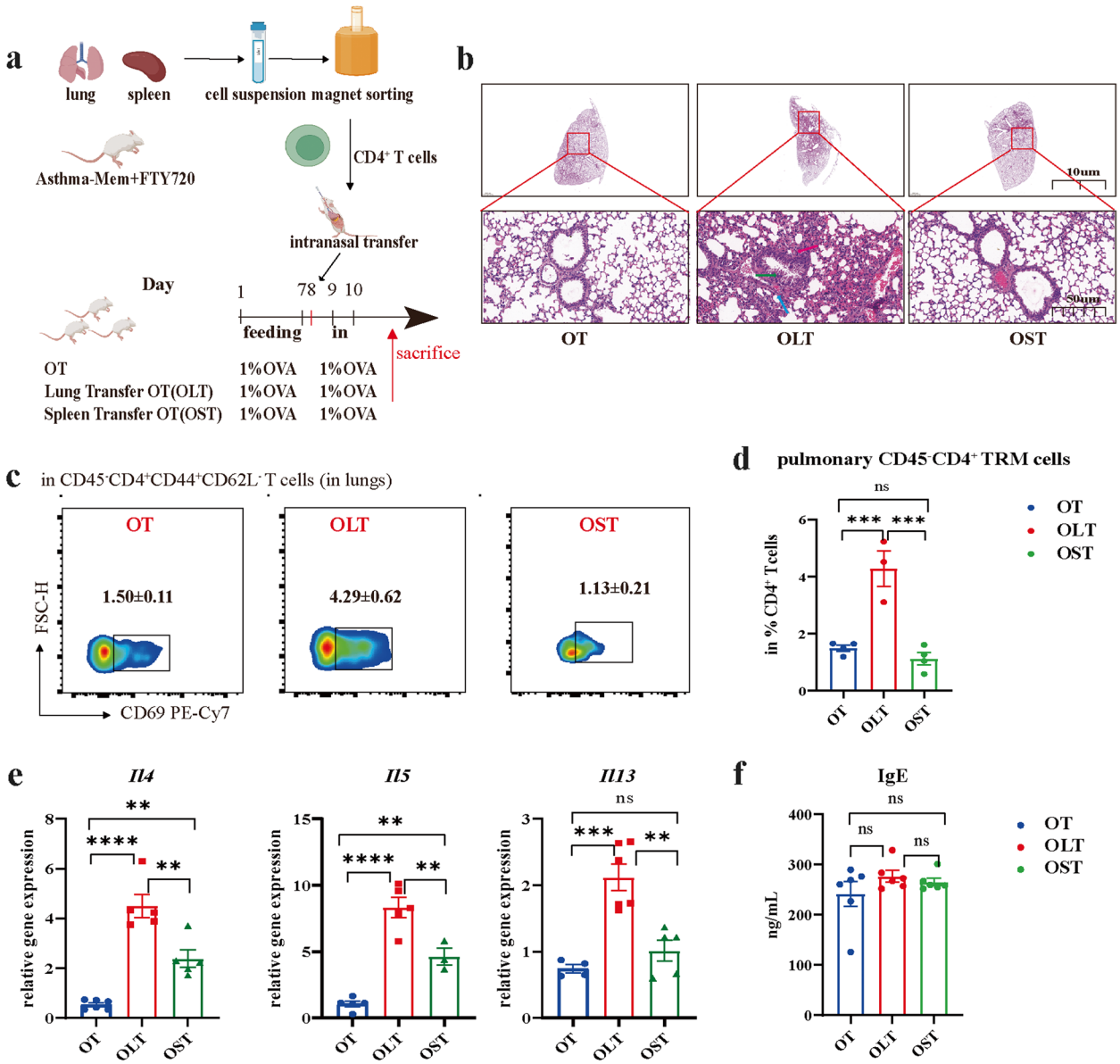

Fig. 5 Transferring CD4$^+$ TRM cells into oral tolerance (OT) mice induces Th2-related inflammation. **a** Workflow of CD4$^+$ T cells in the lung and spleen sorting and adopted transfer of CD4$^+$ TRM cells to OT mice ($n = 4$–6/group). **b** Representative microphotographs of lung histological sections from OT, OLT, and OST groups in objective magnification × 1 and × 20; Green arrow: inflamed airway; Red arrow: inflammatory cell infiltration; Blue arrow: congestive small blood vessels. **c, d** Proportion of pulmonary CD45$^-$CD4$^+$ TRM cells in CD4$^+$ T cells. **e** Type 2 (T2) cytokines including *Il4*, *Il5,* and *Il13* detected by real time qPCR. **f** Plasma IgE secretion detected by ELISA; bars indicate mean ± SEM. Data in **d**, **f** were analyzed using one-way ANOVA. *$P < 0.05$, **$P < 0.01$, ***$P < 0.001$, ****$P < 0.0001$, ns: not significant. OLT: Lung transfer oral tolerance, OST: Spleen transfer oral tolerance, TRM: resident memory T cells, Mem: Memory

demonstrated that CD4$^+$ TRM cells contributed to the disruption of immune tolerance in asthma.

Conditional knockout of PLZF reduces CD4$^+$ TRM cells and relieves asthma symptoms

Since CD4$^+$ TRM cells were fundamental to immune tolerance disruption, we further investigated the regulatory mechanisms underlying the increase in CD4$^+$ TRM cells. Our previous studies demonstrated the critical role of PLZF (encoded by gene *Zbtb16*) in regulating memory phenotypes [35]. PLZF is an important transcription factor involved in the development of tolerance and CD4$^+$ T cell differentiation [36]. Accordingly, we conditionally knocked out *Zbtb16* expression in CD4$^+$ T cells of

C57BL/6 mice (cKO) to generate in vivo pathological and tolerance models (Fig. 6a**,** Fig. S5a–c). Inflammation was significantly relieved, as indicated by reduced immune cell infiltration and decreased airway density, in the asthma cKO mice compared with the WT cKO group (Fig. 6b, c). Consistently, decreased secretion of T2 cytokines was detected in the asthma cKO mice, similar to the lungs of WT-OT model mice (Fig. 6d). Consistently, the eosinophil counts in the BALF of cKO-Asthma mice were markedly decreased compared with WT-Asthma mice (Fig. 6d). Meanwhile, the total number of $CD4^+$ T cells remained stable between asthma groups of the *Zbtb16*-cKO and WT mice, whereas the proportion of $CD4^+CD44^+$ T cells decreased in cKO mice (Fig. 6f**,** Fig. S5e, f). Moreover, a decrease in $CD4^+$ TRM cells and an increase in $CD4^+$ TEM cells was observed in cKO mice (Fig. 6g); the decrease in $CD4^+$TRM cells was confirmed by flow cytometry based on CD45 levels. This was consistent with the reduction in Th2 inflammation in the lungs (Fig. 6h). Similar results were obtained in Asthma-mem mice (Fig. S6). These results suggested a fundamental role for PLZF in $CD4^+$ T cells in directing $CD4^+$ TRM cell differentiation.

PLZF promotes the development of $CD4^+$ TRM cells through the IL-15/IL15 receptor alpha signaling

Multiple signaling pathways, including the IL-7, IL-15, and Notch pathways, participate in regulating $CD4^+$ TRM cell differentiation [37]. Hence, we verified the expression of multiple receptors in the asthmatic lung. The gene expression of *Il7r*, *Dll4*, *Il15ra,* and *Il15rb* was higher in wild-type mice than in cKO mice (Fig. 7a**,** Fig. S7a). Western blotting further confirmed the significantly higher level of IL-15Rα in the asthma group of WT mice (Fig. 7b,Fig. S7b). This suggested that PLZF may potentially regulate the development of $CD4^+$ TRM cells through IL-15/IL-15Rα signaling.

To further explore the role of IL-15/IL-15Rα signaling in regulating PLZF in $CD4^+$ TRM cells, we treated mice with 0.2 mg/kg inbakicept intravenously—an IL-15Rα agonist—in sensitization (day 1) and aerosol (days 7 and 14; Fig. 7c). The increased IL-15Rα activation in cKO-asthmatic mice markedly worsened airway inflammation, breaking the established tolerance (Fig. 7d). T2 cytokine secretion increased markedly, and IgE levels increased slightly in cKO-asthmatic mice treated with inbakicept (Fig. 7e, f). Accordingly, a substantial increase in $CD4^+CD44^+$ T cells was observed, accounting for 85% of the total $CD4^+$ T cell population (Fig. 7g). Furthermore, inbakicept stimulated an increase in $CD4^+$TRM cells, accounting for one-third of $CD4^+$ T cells and approximately half of the $CD4^+CD44^+$ T cell population (Fig. 7h–k). These resulted implied that PLZF expression in $CD4^+$ T cells induced asthmatic inflammation by decreasing $CD4^+$ TRM cells through IL-15/IL-15Rα signaling.

The development of $CD4^+$ memory T cells has been shown to depend on exogenous IL-15 rather than self-secretion, as previously reported [38, 39]. To investigate this, we measured IL-15 secretion in the BALF using ELISA. No statistical difference was observed in the IL-15 levels of BALF between cKO- and WT-asthmatic mice (Fig. 8a). These findings suggest that PLZF likely regulates the responsiveness of IL-15Rα on $CD4^+$ T cells, promoting their responsiveness to IL-15 and differentiation into $CD4^+$ TRM cells, which secrete T2 cytokines. Real-time qPCR analysis revealed significantly higher expression of T2 cytokines, including *Il4, Il5*, and *Il13*, in $CD4^+$ T cells sorted from the lungs of WT-asthmatic mice compared to cKO-asthmatic mice (Fig. 8b).

Furthermore, flow cytometry and immunofluorescence results indicated that pulmonary $CD4^+$ T cells from cKO-asthmatic mice tended to express more IL-15Rα than those from WT-asthmatic mice (Fig. 8c, d). CUT&Tag analysis suggested that PLZF may bind to the *Il15* promoter to regulate its expression (Fig. 8e).

To further explore whether *Zbtb16* knockout in $CD4^+$ T cells reduced IL-15Rα expression and subsequently decreased $CD4^+$ TRM cell differentiation, we sorted pulmonary and splenic lymphocytes from *Zbtb16*-cKO and WT mice and cultured them in vitro (Fig. 8f). No statistical difference was observed in the proportion

(See figure on next page.)

Fig. 6 *Zbtb16* knockout in $CD4^+$ T cells exhibit allergic lung inflammation with decreased $CD45^-CD4^+$ TRM cells. **a** Scheme of asthma and oral tolerance (OT) model in $Zbtb16^{flox/flox}$ $CD4^{Cre}$(cKO) and wild-type C57 mice ($n = 4$–6/group). **b** Representative microphotographs of lung histological sections from Asthma and OT mice in objective magnification × 29; Green arrow: inflamed airway; Red arrow: inflammatory cell infiltration; Blue arrow: congestive small blood vessels. **c** Comparison of lung histological sections from cKO and wildtype Asthma mice at × 1 and × 29 magnification. **d** Differential cell count of bronchoalveolar lavage fluid (BALF) from cKO and WT asthmatic mice. **e** mRNA expression of *Il4, Il5,* and *Il13* in whole lung tissues. **f** Proportion of $CD4^+$ T cells in asthmatic lungs from cKO and wild-type C57 mice. **g** Flow cytometric analysis of pulmonary $CD4^+$ TCM, $CD4^+$ TEM, and $CD4^+$ TRM cells in asthmatic cKO and wild-type C57 mice. **h** Flow cytometric analysis of $CD45^-CD4^+$ TRM cells in lungs of the Asthma group from cKO and wild-type C57; bars indicate mean ± SEM; unpaired two-tailed Student's *t*-test. Data in **d, e, g** were analyzed using one-way ANOVA. $^*P < 0.05$, $^{**}P < 0.01$, $^{***}P < 0.001$, $^{****}P < 0.0001$, ns: not significant. cKO: $Zbtb16^{flox/flox}CD4^{Cre}$, TRM: resident memory T cells

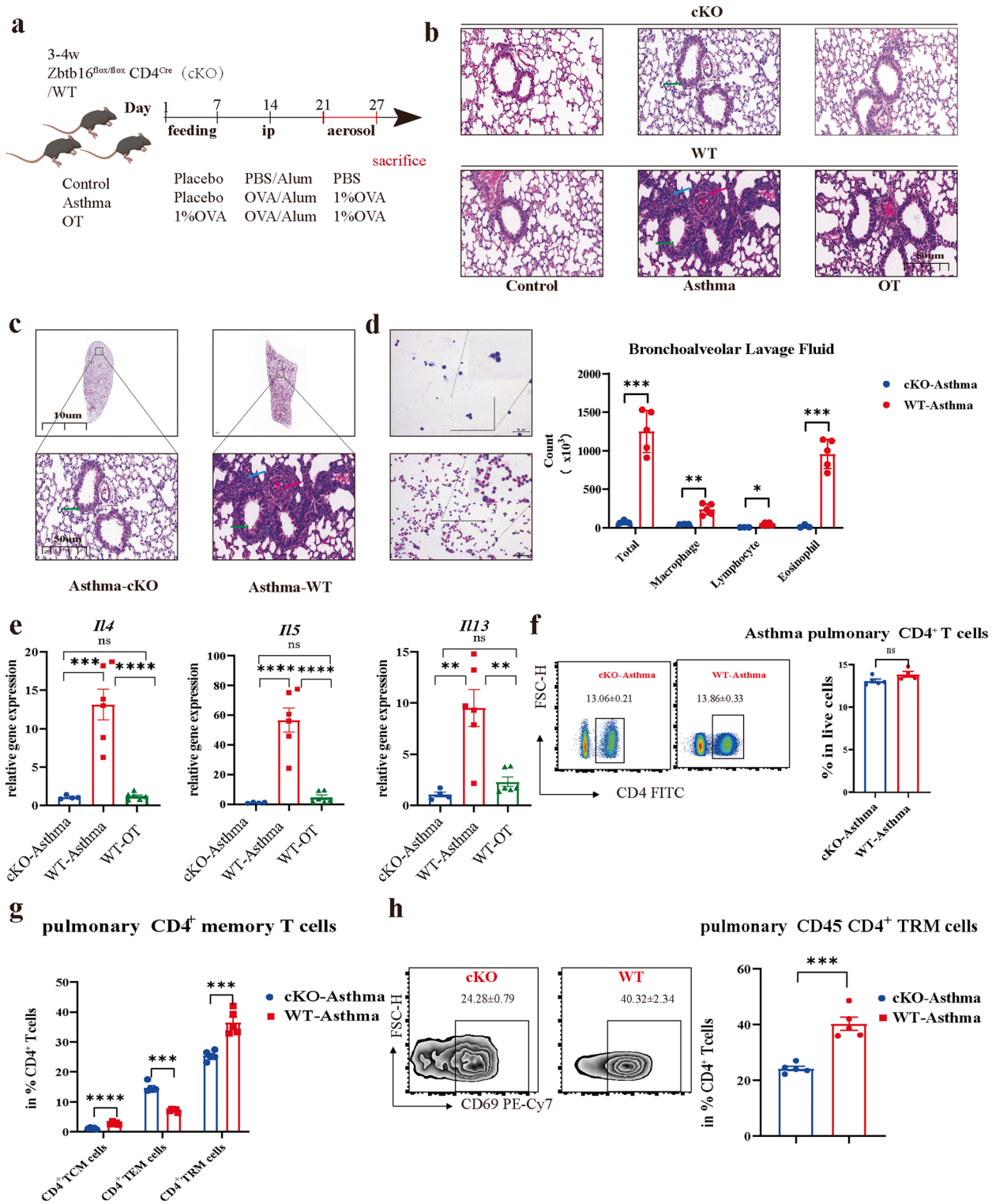

Fig. 6 (See legend on previous page.)

of pulmonary CD4⁺CD44⁺ T cells between cKO and WT mice under basal conditions. However, treatment with OVA-Beas2b effectively increased the number of pulmonary CD4⁺CD44⁺ T cells in cKO and WT cell cultures (Fig. 8g). Notably, co-treatment with IL-15 and OVA-Beas2b significantly increased pulmonary

$CD4^+CD44^+$ T cells in WT cell cultures, not cKO cell cultures. Specifically, the OVA-Beas2b and IL-15 treatment induced more WT $CD4^+$ T cells to differentiate into $CD4^+$ TRM in vitro, whereas cKO $CD4^+$ T cells failed to do so (Fig. 8h). Although splenic cKO $CD4^+$ T cells differentiated into $CD4^+$ TRM cells, the levels were lower than in the WT $CD4^+$ T cell cultures (Fig. 8i).

These findings highlight the critical role of IL-15 in regulating PLZF-mediated $CD4^+$ TRM cell differentiation. IL-15 significantly promotes the differentiation of pulmonary and splenic $CD4^+$ TRM cells. Additionally, downstream proteins JAK1 and JAK3 were more highly expressed in WT $CD4^+$ T cells than cKO $CD4^+$ T cells (Fig. S7d). Hence, PLZF-expressing $CD4^+$ T cells may promote $CD4^+$ TRM cell differentiation through IL-15/IL-15Rα signaling, inducing Th2 responses in allergic airway inflammation.

Discussion

Th2-high asthma is a chronic airway disease ranging in severity from early mild wheezing to life-threatening airway closure [40, 41]. Numerous studies have investigated the mechanisms of asthma to inform the development of targeted drug therapies. While emerging evidence highlights the role of memory T cells in chronic inflammatory processes, current therapeutic strategies increasingly focus on biologics that prevent exacerbations through specific immune pathway modulation. Furthermore, the mechanisms responsible for long-term chronic inflammation remain unclear. Identifying specific targets that mediate long-term inflammation will facilitate the development of novel therapeutic approaches and improve responses to existing therapies.

In this study, we determined the role of $CD4^+$ TRM cells in disrupting immune tolerance and that of the transcription factor PLZF in $CD4^+$ T cells in regulating $CD4^+$ TRM cell differentiation in mouse models of asthma. The results indicate that an increase in the number and function of $CD4^+$ TRM cells promotes the recurrence of early asthmatic pulmonary inflammation and induces Th2-related inflammation in OT to break tolerance. Meanwhile, knocking out PLZF in $CD4^+$ T cells significantly alleviates asthmatic inflammation and decreases the proportion of $CD4^+$ TRM cells. Furthermore, PLZF in $CD4^+$ T cells facilitated $CD4^+$ TRM cell development via IL-15/IL-15Rα signaling.

$CD4^+$ memory T cells are expressed at high levels in the lungs of patients with asthma [19]. Independent of circulating immune memory cells, $CD4^+$ TRM cells are considered to be the primary reactive immune memory cells in the early stage of asthma in an asthmatic mouse model of house dust mites [20, 21] However, the role of $CD4^+$ TRM cells in immune-tolerant lungs has not been reported, with the classification of $CD4^+$ memory T cells incomplete. Our findings are consistent with a recent study indicating that $CD4^+$ TRM cells are highly expressed in asthmatic lungs for at least 6 weeks in BALB/c mice [31, 42]. Consistent differences were observed in the lungs of asthmatic and tolerant mice. Rahimi et al. demonstrated that tissue-resident Th2 cells and circulating memory Th2 cells are functionally and transcriptionally distinct subsets with unique roles in promoting allergic airway inflammation [42]. On the one hand, our results support the conclusion of Rahimi et al. that Th2 TRM cells are critical for local immune responses, as we found that $CD4^+$ TRM cells alone can break immune tolerance in asthma, even in the absence of circulating memory T cells. Furthermore, we found that low antigen concentrations can stimulate asthmatic changes, including increased inflammatory cell infiltration and Th2-related responses, consistent with the functional role of Th2 TRM cells described by Rahimi et al. On the other hand, our findings regarding circulating memory T cells differ from those of Rahimi et al. This discrepancy could be attributed to our focus on the critical role of TRM cells in asthma reactivation, while Rahimi et al. highlighted the synergistic roles of circulating and resident memory T cells. They also identified that TRM cells play a more prominent role during the early stages of asthma reactivation compared to circulating memory T cells. Circulating memory T cells have functional capabilities; however, their response appears to be delayed compared to the rapid activation of tissue-resident TRM cells. Moreover, unlike Rahimi et al., we did not distinguish between Th1 and Th2 subsets of

(See figure on next page.)

Fig. 7 PLZF in $CD4^+$ TRM cells decreases asthma-related Th2 inflammation via IL15/IL15Rα signaling. **a** *Il15*ra mRNA expression. **b** IL15Rα protein expression in control, asthmatic, and tolerant lungs from cKO and wild-type C57 mice. **c** IL15Rα agonist, Inbakicept, was used for the 1st sensitization, the 7th and 14th of 1% OVA aerosol ($n = 4$–6/group). **d** Comparison of lung histological sections from cKO inbakicept-treated and untreated asthmatic mice at × 1 and × 29 magnification. **e** mRNA expression levels of *Il4*, *Il5*, and *Il13* in the whole lungs. **f** Plasma IgE levels assessed by ELISA. **g** Comparison of $CD4^+CD44^+$ T cells in the lungs. **h, i** Proportion of $CD4^+$ TCM, $CD4^+$ TEM, and $CD4^+$ TRM cells in the lung $CD4^+$ T cells. **j** Proportion of $CD4^+$ TCM, $CD4^+$ TEM, and $CD4^+$ TRM cells in the lung $CD4^+CD44^+$ T cells. **k** Flow cytometric analysis of $CD45^-CD4^+$ TRM cells in lungs; bars indicate mean ± SEM. Data in **a**, **b** were analyzed using one-way ANOVA and data in **e**, **f** were analyzed using unpaired two-tailed Student's *t*-test. *$P < 0.05$, **$P < 0.01$, ***$P < 0.001$, ****$P < 0.0001$, ns: not significant. cKO: $Zbtb16^{flox/flox}CD4^{Cre}$

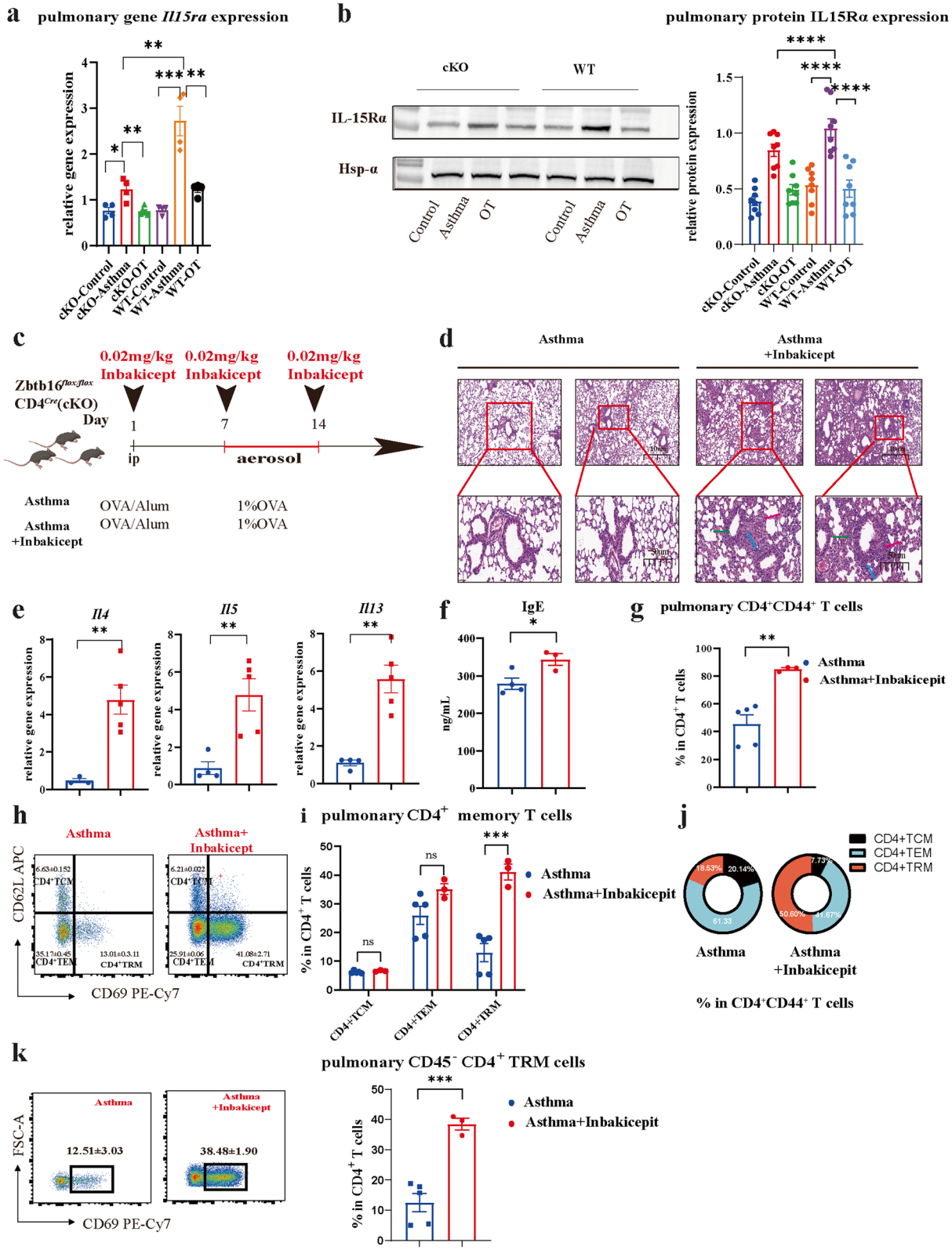

Fig. 7 (See legend on previous page.)

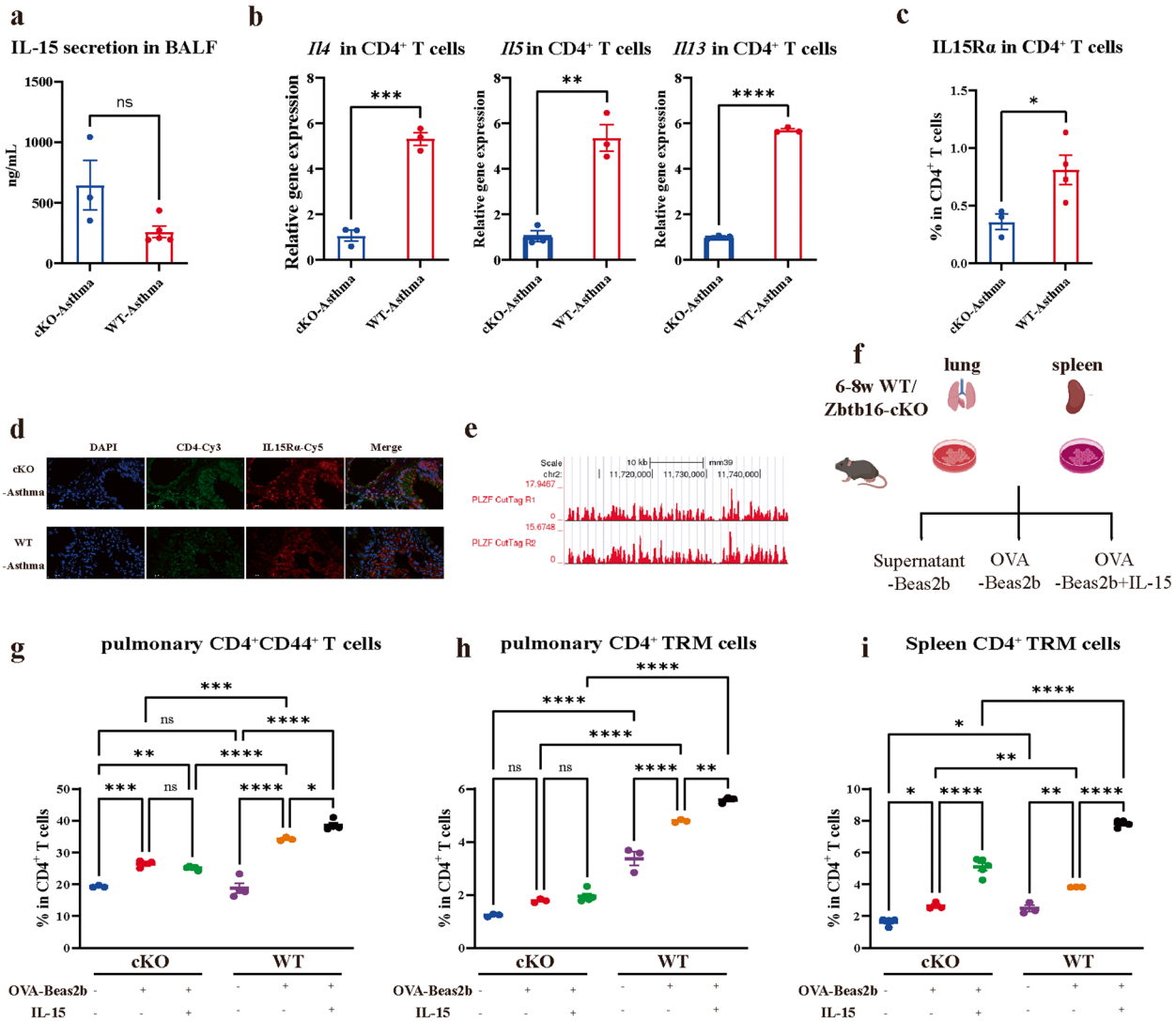

Fig. 8 PLZF in CD4$^+$ T cells can increase CD4$^+$ TRM cells through upregulate IL15Rα on CD4$^+$ T cells. **a** Comparison of IL-15 in the BALF from cKO and WT asthmatic mice by ELISA. **b** Gene expression levels of Il4, Il5, and Il13 in the CD4$^+$ T cells forted from the lungs assessed by real-time qPCR. **c** Comparison of IL15Rα in CD4$^+$ T cells from the lungs of cKO and WT mice by flow cytometry. **d** Representative confocal images of lungs from cKO-Asthma and WT-Asthma mice with labeled CD4-Cy3 (green), IL15Rα (red) and DAPI (blue) in objective magnification × 20. Scale bar represents 50 μm. **e** CUT&Tag analysis of PLZF in sorted CD4$^+$ T cells using anti-PLZF antibody shows enrichment at IL15Rα. f Workflow of pulmonary and splenic lymphocytes sorted and stimulated by OVA-Beas2b as well as IL-15 in vitro. g Comparison of pulmonary CD4 + CD44 + T cells stimulated in vitro. h,i Comparison of pulmonary and splenic CD4 + TRM cells. All bars in this figure indicate mean + / − SEM. Data in **a**,**d**,**e** were analyzed using unpaired two-tailed Student's t test and data in **g**,**h**,**i** were analyzed using one way ANOVA test. *$P < 0.05$, **$P < 0.01$, ***$P < 0.001$, ****$P < 0.0001$, ns: not significant. BALF: Bronchoalveolar Lavage Fluid, TRM: tissue resident memory T cells

circulating memory T cells (e.g., CD4$^+$ TEM and CD4$^+$ TCM cells), which may account for the lack of differences within the circulating memory T cells in our model. We are conducting follow-up studies to further explore the roles of different TRM cell subsets to provide additional insights into their contributions to asthma pathogenesis.

PLZF, encoded by the *Zbtb16* gene, belongs to the BTB-ZF family of transcription factors, with critical regulatory roles in cell proliferation, development, and organ differentiation [43]. Our previous study on asthma and OT models revealed that invariant natural killer T (iNKT) cells with high PLZF expression are recruited into lung tissue to aid in inducing immune tolerance [40]. Moreover, PLZF$^+$CD4$^+$ T cells in lymphocytes and the spleen increase the proliferative capacity of Foxp3$^+$CD4$^+$ "natural" Tregs through IL-4, generating activated/memory-like regulatory T cells [44]. Furthermore, human CD4$^+$ T cells expressing PLZF exhibit the characteristics

of terminally differentiated effector memory $CD4^+$ T cells [36].

Knockdown of PLZF expression in $CD4^+$ T cells significantly reduced the proportion of $CD4^+$ TRM cells. Moreover, allergic lung inflammation, including the release of airway contraction products and T2-related cytokines (IL-4, IL-5, and IL-13), was reduced in Zbtb16-cKO mice. These findings contradict a previous study in which PLZF promoted immune tolerance by downregulating the memory phenotype and decreasing $CD4^+$ TEM and $CD4^+$ TCM cell proportions [35]. This discrepancy may originate from two potential sources. First, PLZF may exert unique roles in different cell types. PLZF may promote the recruitment of iNKT cells to induce immune tolerance, whereas in $CD4^+$ T cells, it may exploit disparate functions, inducing characteristics of tissue-resident memory $CD4^+$ T cells. However, the effect of PLZF depends on its functional composition. For example, Li et al. knocked out or overexpressed PLZF in all splenic lymphocytes, revealing that PLZF influences the memory phenotype CD44 and CD62L, which differs from the effect of PLZF knockdown in $CD4^+$ T cells. Second, the classification may differ markedly; Li et al. focused on circulating memory T cells like $CD4^+$ TEM and $CD4^+$ TCM cells. At this point, our research makes a more detailed distinction in the memory T cells including $CD4^+$ TEM, $CD4^+$ TCM and $CD4^+$ TRM cells. Furthermore, we found that $CD4^+$ T cells expressing PLZF could enhance the differentiation of $CD4^+$ TRM cells through IL-15/IL-15Rα signaling. Interleukins such as IL-15 and IL-2 facilitate the differentiation of $CD4^+$ TRM cells in asthmatic mouse models [21, 45]. Unfortunately, the downstream regulation of PLZF in $CD4^+$ T cells directed by IL-15/IL-15Rα remains unknown.

IL-15, traditionally classified as a type 1 alarmin due to its role in activating NK cells and $CD8^+$ T cells, has also been implicated in type 2 inflammation under specific conditions. For instance, IL-15 promotes Th2 cell proliferation, differentiation, and IL-5 production in vitro; however, these effects require co-stimulation with IL-4, highlighting its auxiliary role in type 2 immunity [46]. Additionally, IL-15 can modulate the activity of innate lymphoid cells (ILCs), particularly ILC2s, which are key drivers of type 2 inflammation through IL-5 production. Although IL-15 does not directly induce type 2 cytokines, it may influence the inflammatory environment to affect ILC2 function [47]. IL-15 may also play a role in the type 2 responses of asthma, as the lungs of wild-type asthma mice showed higher expression of IL-15Rα compared to *Zbtb16*-cKO mice in the current study. Furthermore, the use of an IL-15Rα agonist, inbakicept, significantly increased allergic airway inflammation and T2 cytokine secretion. However, these findings differ from previous studies on IL-15. For example, in allergen-induced airway obstruction models, Venkateshaiah et al. found that IL-15 deficiency worsened airway resistance and reduced lung compliance, whereas IL-15 overexpression improved lung function by reducing pro-inflammatory cytokine levels (e.g., IL-4, IL-5, IL-13) and increasing anti-inflammatory IL-10 [48]. Additionally, IL-15 agonists like ALT-803 have shown therapeutic potential by relieving airway obstruction and mucus secretion. From our perspective, three potential explanations may account for these discrepancies. First, although IL-15 does not directly drive type 2 responses in asthma, it may indirectly promote type 2 inflammation under specific conditions. Second, IL-15 concentration is critical in regulating inflammation. At low concentrations, IL-15 maintains immune cell homeostasis by regulating survival, proliferation, and metabolism through the JAK/STAT, PI3K/AKT, and MAPK pathways; however, at high concentrations, IL-15 drives inflammation and autoimmunity by promoting cytotoxicity and dysregulated immune responses, leading to tissue damage [49]. Third, IL-15 can promote IFN-γ and other pro-inflammatory cytokines to create a mixed inflammatory environment, amplifying chronic inflammatory responses where type 1 and 2 pathways coexist, as in asthma [50]. Despite these findings, the precise mechanisms by which IL-15 influences type 2 inflammation remain unclear. Further research is needed to clarify its role and therapeutic potential in diseases involving type 1 and 2 immune responses.

Our study provides novel insights into the role of $CD4^+$ TRM cells in the breakdown of immune tolerance in asthma, highlighting their critical involvement in the pathogenesis of allergic airway inflammation. While previous studies have primarily focused on circulating memory T cells (e.g., $CD4^+$ TEM and TCM cells) in asthma exacerbations, our research uniquely emphasizes the dominant role of $CD4^+$ TRM cells in driving local immune responses and reactivating asthma. By employing both asthma and OT mouse models, we demonstrate that $CD4^+$ TRM cells alone are sufficient to induce allergic inflammation in the tolerance mice, even in the absence of circulating memory T cells. This finding underscores the pivotal role of TRM cells in the early stages of asthma reactivation, distinguishing their function from that of circulating memory T cells. Furthermore, this study is the first to elucidate the regulatory role of PLZF in $CD4^+$ TRM cells during asthma immune tolerance. Through a quantitative proteomic approach, we reveal that PLZF expression in $CD4^+$ T cells enhance the development and maintenance of $CD4^+$ TRM cells, which subsequently disrupt immune tolerance via the IL-15/

IL-15Rα signaling pathway. While PLZF has been previously implicated in the regulation of memory T cells, our study provides a more detailed mechanistic understanding of its role in tissue-resident memory subsets, particularly in the context of asthma. This expands the current understanding of PLZF beyond its established functions in iNKT cells and circulating memory T cells.

The current study has certain limitations. First, two different mouse strains (BALB/c and C57BL/6) were employed, potentially introducing variability due to their distinct immune characteristics. BALB/c mice are known for their Th2-skewed immune responses, whereas C57BL/6 mice exhibit less significant Th2-biased responses, potentially influencing the immune mechanisms. Although the differences in genetic background might affect the generalizability of specific findings, we have validated our conclusions across both strains. Moreover, the use of both strains reinforces the generalizability of our conclusions. Future studies should focus on standardizing experimental models or exploring strain-specific differences to further clarify these mechanisms and their implications for human asthma. Second, this study did not explore potential therapeutic drugs or compounds that specifically target PLZF in $CD4^+$ T cells. Further research is needed to investigate whether modulating PLZF activity in these cells could serve as a viable strategy for therapeutic intervention in asthma. Also, experiments on human specimen are also critical for the potential application.

Conclusions

This study underscores the importance of $CD4^+$ TRM cells in the pathogenesis of asthma and suggests that targeting the PLZF and IL-15/IL-15Rα signaling pathways could offer new avenues for treating long-term asthmatic inflammation. $CD4^+$ TRM cells are vital pathogenic factors involved in the breakdown of immune tolerance to induce asthma. Meanwhile, knocking down PLZF in $CD4^+$ T cells induces immune tolerance through IL-15/IL15Rα signaling. Utilizing appropriate ligands to specifically target PLZF in $CD4^+$ T cells may reveal new targeted therapies, offering significant potential for asthma clinical treatments.

Abbreviations

cKO	$Zbtb16^{flox/flox}CD4^{Cre}$
BALF	Bronchoalveolar lavage fluid
i.n.	Intranasal
i.p.	Intraperitoneal
Mem	Memory
OLT	Lung transfer oral tolerance
OST	Spleen transfer oral tolerance
OT	Oral tolerance
OVA	Ovalbumin
PLZF	Promyelocytic leukemia zinc finger
PVDF	Polyvinylidene difluoride
TCM	Central memory T cells
TEM	Effector memory T cells
TRM	Resident memory T cells
WT	Wildtype

Supplementary Information

The online version contains supplementary material available at https://doi.org/10.1186/s12964-025-02134-x.

Supplementary Material 1. Fig. S1 Splenic $CD4^+CD44^+$ T cells and $CD4^+$ TCM cells do not differ among asthmatic and tolerant mice. a, b PAS and Masson trichrome analysis of the lungs from control, asthma, and oral tolerancemice c, d Proportion of pulmonary and splenic $CD4^+CD44^+$ cells in $CD4^+$ T cells. e, f Flow cytometric analysis of $CD4^+$TCM, $CD4^+$TEM, and $CD4^+$TRM cells in the spleens of control, asthmatic, and OT mice; bars indicate mean ± SEM. Data in d, f were analyzed using one-way ANOVA. $^*P < 0.05$, $^{**}P < 0.01$, $^{***}P < 0.001$, $^{****}P < 0.0001$, ns: not significant. PAS: Periodic acid-Schiff, TCM: central memory T cells, TEM: effector memory T cells, TRM: resident memory T cells. Fig. S2 Relapsed lung Th2-related inflammation in allergic lungs with highly abundant $CD4^+CD44^+$T cells, especially $CD4^+$TRM cells. a Representative microphotographs of lung histological sections from Control-mem, Asthma-mem, and oral tolerance-mem mice under × 29 objective magnification on days 28, 35, 42, 49, 56, 63,71, 78, and 85; Green arrow: inflamed airway; Red arrow: inflammatory cell infiltration; Blue arrow: congestive small blood vessels. b mRNA expression of *Il4, Il5,* and *Il13* in the whole lung tissues. c Proportion of pulmonary $CD4^+CD44^+$ T cells in live cells. d Flow cytometric analysis of $CD4^+$TEM and $CD4^+$TRM cells in the lungs of Control-mem, Asthma-mem, and OT-mem mice; bars indicate mean ± SEM. Data in b, c, d were analyzed using one-way ANOVA. $^*P < 0.05$, $^{**}P < 0.01$, $^{***}P < 0.001$, $^{****}P < 0.0001$, ns: not significant. TCM: central memory T cells, TEM: effector memory T cells, TRM: resident memory T cells, Mem: Memory Fig. S3 Successful separation of $CD4^+$T cells. a Flow cytometric analysis of gradient centrifugation efficiency in $CD45^+$ and T cells. b Flow cytometric analysis of magnet bead sorting efficiency in T cells and $CD4^+$ T cell; bars indicate mean ± SEM. Data in c, d, f, h were analyzed using unpaired two-tailed Student's *t*-test. $^*P < 0.05$, $^{**}P < 0.01$, $^{***}P < 0.001$, $^{****}P < 0.0001$, ns: not significant. Fig. S4 Proportions of separated $CD4^+$TRM cells in lungs increase through gradient centrifugation and magnetic sorting. a Flow cytometric sorting pathway to classify the $CD4^+$TCM, $CD4^+$TEM, and $CD4^+$ TRM cells. b, c Flow cytometric analysis of combined gradient centrifugation and magnet bead sorting efficiency in T cells, $CD4^+$T cells, $CD4^+CD44^+$T cells, and $CD4^+$memory T cells based on target cell estimation in total live cells of lungs and spleens. Bars indicate mean ± SEM. Data in b, c were analyzed using unpaired two-tailed Student's *t*-test. $^*P < 0.05$, $^{**}P < 0.01$, $^{***}P < 0.001$, $^{****}P < 0.0001$, ns: not significant. TCM: central memory T cells, TEM: effector memory T cells, TRM: resident memory T cells. Fig. S5 Successful knockout of *Plzf* in $CD4^+$ T cells markedly decreases $CD4^+CD44^+$ T cells. a Representative confocal image of lungs from cKO and wild-type mice with CD4-Cy3, PLZF-FITC, and DAPIunder ×20 objective magnification; Scale bar, 50 μm; Circles: $PLZF^+CD4^+$T cells. b, c Flow cytometric analysis of the proportion of PLZF in $CD4^+$ T lung cells from cKO and wild-type mice. d $CD45^-CD4^+$ TRM cell proportion in the lungs of control, asthma, and OT mice from cKO and wild-type mice detected by flow cytometry. e Comparison of $CD4^+CD44^+$ T cells in asthmatic lungs from cKO and wild-type mice. Bars indicate mean ± SEM. Data in c, f were analyzed using unpaired two-tailed Student's *t*-test and data in d were analyzed using one-way ANOVA. $^*P < 0.05$, $^{**}P < 0.01$, $^{***}P < 0.001$, $^{****}P < 0.0001$, ns: not significant. cKO: $Zbtb16^{flox/flox}CD4^{Cre}$, WT: wild-type, OT: oral tolerance. Fig. S6 $CD45^-CD4^+$TRM cells expressed in wild-type Asthma-mem mice with enhanced lung inflammation. a Comparison of lung histological sections from the lungs of cKO and wild-type Control-mem, Asthma-mem, and oral tolerance-mem mice under 29× objective magnification. Green arrow: inflamed airway; Red arrow: inflammatory cell infiltration; Blue arrow: congestive small blood vessels b $CD45^-CD4^+$TRM cell expression in the lungs of Asthma-mem mice from cKO and wild-type mice detected by flow cytometry. Bars indicate mean ± SEM. Data in b were analyzed using unpaired two-tailed Student's *t*-test.$^*P < 0.05$, $^{**}P$

< 0.01, ***P < 0.001, ****P< 0.0001, ns: not significant. cKO: Zbtb16$^{flox/flox}$CD4^{Cre}, WT: wild-type, TRM: tissue resident memory T cells. Fig. S7 IL-15, IL-7, and Notch gene and protein expression in conditional knockoutand wild-type mice. a mRNA expression of *Il15ra, Dll4, Jagged2, Il7r,* and *Il15rb* in the whole lung. b Abundance of IL-15Rα, DLL4, JAG2, IL-7R, and IL-15Rβ proteins in the whole lungs. c JAK1 and JAK3 protein expression in the CD4$^+$ T cells sorted from the lungs of cKO and wild-type asthmatic mice. Scale bar, 50 μm; bars indicate mean ± SEM. Data in a were analyzed using one-way ANOVA. *P< 0.05, **P < 0.01, ***P < 0.001, ****P < 0.0001, ns: not significant. cKO: Zbtb16$^{flox/flox}$CD4^{Cre}, WT: wild-type, OT: oral tolerance. Fig. S8 Flow cytometric analysis of CD4$^+$TCM, CD4$^+$TEM, and CD4$^+$ TRM cells. a Selection of living mononuclear cells with side scatter/forward scatter. R1 gate was used to select the cells with light scatter properties characteristic of live cells. b R2 gate was used to select the CD4$^+$TCM, CD4$^+$TEM, and CD4$^+$ TRM cells. c, d Detection of CD45$^-$CD4$^+$TRM and CD45$^+$CD4$^+$TEM cell phenotypes following intra-tail injection of anti-CD45 to distinguish resident and circulating cells. CD45$^-$: resident cells, CD45$^+$: circulating cells, cKO: Zbtb16$^{flox/flox}$CD4^{Cre}, WT: wild-type, OT: oral tolerance, TEM: effector memory T cells, TRM: resident memory T cells

Acknowledgements
Not applicable.

Authors' contributions
MZ performed the experiments, interpreted the data, and wrote the manuscript. MZ, SCT, NL and TYS designed the flow cytometry panels and performed the related analysis. SCT, JJF and TYS provided technical support for the magnet beads sorting. SJF, XTR, YXY and ZFM assisted the primary statistical analysis. ZJJ guided the experiments design. ZJJ and SCT revised the manuscript.

Funding
This work was supported by the grants from the National Natural Science Foundation of China (NSFC) (No. 82470019), the construction plan of key disciplines in Shanghai Municipal Health System (No. 2024ZDXK0017), the Specialized Department Foundation of Traditional Chinese Medicine of the 'Fourteenth Five-Year Plan' of Shanghai (No. ZYTSZK1-05), the Key Public Health Discipline Foundation of Minhang District (No. MGWXK2023-01) and the 14th Five-Year National Key R&D Program 'Research on Pathogeny and Epidemic Prevention Technology System' Major Project (No. 2023YFC2307200).

Data availability
No datasets were generated or analysed during the current study.

Declarations

Ethics approval and consent to participate
All the animal experiments were approved by the Committees on Animal Research of the Institute of Immunology and Infection of Shanghai, Chinese Academy of Sciences (Animal Ethics Review Number: 2020088).

Consent for publication
The authors declare that they have no competing interests.

Competing interest
The authors declare no competing interests.

Author details
[1]Department of Pulmonary and Critical Care Medicine, Shanghai Fifth People's Hospital, Fudan University, Shanghai, China. [2]Shanghai Center for Systems Biomedicine, Key Laboratory of Systems Biomedicine (Ministry of Education), Shanghai Jiao Tong University, Shanghai, China. [3]School of Biomedical Engineering, Med-X Research Institute, Shanghai Jiao Tong University, Shanghai, China. [4]Department of Medicine, Respiratory, Emergency and Intensive Care Medicine, The Affiliated Dushu Lake Hospital of Soochow University, Suzhou, China. [5]Center of Community-Based Health Research, Fudan University, Shanghai, China.

Received: 23 September 2024 Accepted: 28 February 2025
Published online: 15 March 2025

References

1. Papi A, Brightling C, Pedersen SE, Reddel HK. Asthma. Lancet. 2018;391:783–800.
2. Krishnamoorthy N, Khare A, Oriss TB, Raundhal M, Morse C, Yarlagadda M, Wenzel SE, Moore ML, Peebles RS, Ray A, Ray P. Early infection with respiratory syncytial virus impairs regulatory T cell function and increases susceptibility to allergic asthma. Nat Med. 2012;18:1525–30.
3. Roychoudhuri R, Hirahara K, Mousavi K, Clever D, Klebanoff CA, Bonelli M, Sciumè G, Zare H, Vahedi G, Dema B, et al. BACH2 represses effector programs to stabilize T(reg)-mediated immune homeostasis. Nature. 2013;498:506–10.
4. Verhasselt V, Milcent V, Cazareth J, Kanda A, Fleury S, Dombrowicz D, Glaichenhaus N, Julia V. Breast milk-mediated transfer of an antigen induces tolerance and protection from allergic asthma. Nat Med. 2008;14:170–5.
5. Tosca MA, Olcese R, Licari A, Ciprandi G. Allergen immunotherapy and asthma. Pediatr Allergy Immunol. 2020;31(Suppl 24):46–8.
6. Eljaszewicz A, Ruchti F, Radzikowska U, Globinska A, Boonpiyathad T, Gschwend A, Morita H, Helbling A, Arasi S, Kahlert H, et al. Trained immunity and tolerance in innate lymphoid cells, monocytes, and dendritic cells during allergen-specific immunotherapy. J Allergy Clin Immunol. 2021;147:1865–77.
7. Penagos M, Durham SR. Allergen immunotherapy for long-term tolerance and prevention. J Allergy Clin Immunol. 2022;149:802–11.
8. Uto T, Takagi H, Fukaya T, Nasu J, Fukui T, Miyanaga N, Arimura K, Nakamura T, Choijookhuu N, Hishikawa Y, Sato K. Critical role of plasmacytoid dendritic cells in induction of oral tolerance. J Allergy Clinical Immunology. 2018;141:2156.
9. Harb H, Stephen-Victor E, Crestani E, Benamar M, Massoud A, Cui Y, Charbonnier L-M, Arbag S, Baris S, Cunnigham A, et al. A regulatory T cell Notch4-GDF15 axis licenses tissue inflammation in asthma. Nat Immunol. 2020;21:1359–70.
10. Sethi GS, Gracias D, Croft M. Contribution of circulatory cells to asthma exacerbations and lung tissue-resident CD4 T cell memory. Front Immunol. 2022;13: 951361.
11. Sethi GS, Gracias DT, Gupta RK, Carr D, Miki H, Da Silva AR, Croft M. Anti-CD3 inhibits circulatory and tissue-resident memory CD4 T cells that drive asthma exacerbations in mice. Allergy. 2023;78:2168–80.
12. Schenkel JM, Masopust D. Tissue-resident memory T cells. Immunity. 2014;41:886–97.
13. Zheng MZM, Wakim LM. Tissue resident memory T cells in the respiratory tract. Mucosal Immunol. 2022;15:379–88.
14. Steinbach K, Vincenti I, Merkler D. Resident-memory T cells in tissue-restricted immune responses: for better or worse? Front Immunol. 2018;9: 2827.
15. Kumar BV, Ma W, Miron M, Granot T, Guyer RS, Carpenter DJ, Senda T, Sun X, Ho S-H, Lerner H, et al. Human tissue-resident memory T cells are defined by core transcriptional and functional signatures in lymphoid and mucosal sites. Cell Rep. 2017;20:2921–34.
16. Mueller SN, Gebhardt T, Carbone FR, Heath WR. Memory T cell subsets, migration patterns, and tissue residence. Annu Rev Immunol. 2013;31:137–61.
17. Goplen NP, Huang S, Zhu B, Cheon IS, Son YM, Wang Z, Li C, Dai Q, Jiang L, Sun J. Tissue-resident macrophages limit pulmonary CD8 resident memory T cell establishment. Front Immunol. 2019;10: 2332.
18. Masopust D, Soerens AG. Tissue-resident T cells and other resident leukocytes. Annu Rev Immunol. 2019;37:521–46.
19. Herrera-De La Mata S, Ramírez-Suástegui C, Mistry H, Castañeda-Castro FE, Kyyaly MA, Simon H, Liang S, Lau L, Barber C, Mondal M, et al. Cytotoxic CD4+ tissue-resident memory T cells are associated with asthma severity. Med. 2023;4:875.
20. Turner DL, Goldklang M, Cvetkovski F, Paik D, Trischler J, Barahona J, Cao M, Dave R, Tanna N, D'Armiento JM, Farber DL. Biased generation and in situ activation of lung tissue-resident memory CD4 T cells in the pathogenesis of allergic asthma. Journal of Immunology. 2018;200:1561–9.

21. Hondowicz BD, An D, Schenkel JM, Kim KS, Steach HR, Krishnamurty AT, Keitany GJ, Garza EN, Fraser KA, Moon JJ, et al. Interleukin-2-dependent allergen-specific tissue-resident memory cells drive asthma. Immunity. 2016;44:155–66.
22. Tabor DE, Fernandes F, Langedijk AC, Wilkins D, Lebbink RJ, Tovchigrechko A, Ruzin A, Kragten-Tabatabaie L, Jin H, Esser MT, et al. Global molecular epidemiology of respiratory syncytial virus from the 2017–2018 INFORM-RSV study. Journal of Clinical Microbiology. 2020;59:e01828.
23. Li H, Bradbury JA, Edin ML, Gruzdev A, Li H, Graves JP, DeGraff LM, Lih FB, Feng C, Wolf ER, et al. TXA2 attenuates allergic lung inflammation through regulation of Th2, Th9, and Treg differentiation. The Journal of Clinical Investigation. 2024;134:134.
24. Ha EH, Choi JP, Kwon HS, Park HJ, Lah SJ, Moon KA, Lee SH, Kim I, Cho YS. Endothelial Sox17 promotes allergic airway inflammation. The Journal of Allergy and Clinical Immunology. 2019;144:561.
25. Kinnear E, Lambert L, McDonald JU, Cheeseman HM, Caproni LJ, Tregoning JS. Airway T cells protect against RSV infection in the absence of antibody. Mucosal Immunol. 2018;11:290.
26. Paik DH, Farber DL. Influenza infection fortifies local lymph nodes to promote lung-resident heterosubtypic immunity. J Exp Med. 2021;218:e20200218.
27. Anderson KG, Mayer-Barber K, Sung H, Beura L, James BR, Taylor JJ, Qunaj L, Griffith TS, Vezys V, Barber DL, Masopust D. Intravascular staining for discrimination of vascular and tissue leukocytes. Nat Protoc. 2014;9:209–22.
28. Guvenel A, Jozwik A, Ascough S, Ung SK, Paterson S, Kalyan M, Gardener Z, Bergstrom E, Kar S, Habibi MS, et al. Epitope-specific airway-resident CD4+ T cell dynamics during experimental human RSV infection. J Clin Investig. 2020;130:523–38.
29. Mims JW. Asthma: definitions and pathophysiology. International Forum of Allergy & Rhinology. 2015;5(Suppl 1):S2–6.
30. Hammad H, Lambrecht BN. The basic immunology of asthma. Cell. 2021;184:2521–2.
31. Bošnjak B, Kazemi S, Altenburger LM, Mokrović G, Epstein MM. Th2-TRMs maintain life-long allergic memory in experimental asthma in mice. Front Immunol. 2019;10: 840.
32. Raphael I, Joern RR, Forsthuber TG. Memory CD4+ T cells in immunity and autoimmune diseases. Cells. 2020;9:531.
33. Reilly EC, Lambert Emo K, Buckley PM, Reilly NS, Smith I, Chaves FA, Yang H, Oakes PW, Topham DJ. TRM integrins CD103 and CD49a differentially support adherence and motility after resolution of influenza virus infection. Proc Natl Acad Sci USA. 2020;117:12306–14.
34. Van Braeckel-Budimir N, Varga SM, Badovinac VP, Harty JT. Repeated Antigen exposure extends the durability of influenza-specific lung-resident memory CD8+ T Cells and heterosubtypic immunity. Cell Reports. 2018;24:3374.
35. Li N, Shi T, Zhang M, He Y, Feng J, Mei Z, Su X, Jie Z. PLZF promotes the development of asthma tolerance via affecting memory phenotypes of immune cells. Int Immunopharmacol. 2023;114: 109559.
36. Kim Y-H, Zhu L, Pyaram K, Lopez C, Ohye RG, Garcia JV, Green GE, Chang C-H. PLZF-expressing CD4 T cells show the characteristics of terminally differentiated effector memory CD4 T cells in humans. Eur J Immunol. 2018;48:1255–7.
37. Zhang M, Li N, He Y, Shi T, Jie Z. Pulmonary resident memory T cells in respiratory virus infection and their inspiration on therapeutic strategies. Front Immunol. 2022;13: 943331.
38. Waickman AT, Ligons DL, Hwang S, Park J-Y, Lazarevic V, Sato N, Hong C, Park J-H. CD4 effector T cell differentiation is controlled by IL-15 that is expressed and presented in trans. Cytokine. 2017;99:266–74.
39. Purton JF, Tan JT, Rubinstein MP, Kim DM, Sprent J, Surh CD. Antiviral CD4+ memory T cells are IL-15 dependent. J Exp Med. 2007;204:951–61.
40. Tesfaye ZT, Gebreselase NT, Horsa BA. Appropriateness of chronic asthma management and medication adherence in patients visiting ambulatory clinic of Gondar University Hospital: a cross-sectional study. The World Allergy Organization Journal. 2018;11:18.
41. Toumpanakis D, Usmani OS. Small airways in asthma: pathophysiology, identification and management. Chinese Medical Journal Pulmonary and Critical Care Medicine. 2023;1:171–80.
42. Rahimi RA, Nepal K, Cetinbas M, Sadreyev RI, Luster AD. Distinct functions of tissue-resident and circulating memory Th2 cells in allergic airway disease. The Journal of Experimental Medicine. 2020;217:e20190865.
43. Zhang Q, Li X, Li Y, Chen S, Shen X, Dong X, Song Y, Zhang X, Huang K. Expression of the PTEN/FOXO3a/PLZF signalling pathway in pancreatic cancer and its significance in tumourigenesis and progression. Invest New Drugs. 2020;38:321–8.
44. Feng X, Zhao C, Li L, Feng J, He W, Shi T, Li N, Jie Z, Su X. iNKT cells with high PLZF expression are recruited into the lung via CCL21-CCR7 signaling to facilitate the development of asthma tolerance in mice. Eur J Immunol. 2021;51:414–32.
45. Strutt TM, Dhume K, Finn CM, Hwang JH, Castonguay C, Swain SL, McKinstry KK. IL-15 supports the generation of protective lung-resident memory CD4 T cells. Mucosal Immunol. 2018;11:668–80.
46. Niedbala W, Wei X, Liew FY. IL-15 induces type 1 and type 2 CD4+ and CD8+ T cells proliferation but is unable to drive cytokine production in the absence of TCR activation or IL-12 / IL-4 stimulation in vitro. Eur J Immunol. 2002;32:341–7.
47. Robinette ML, Bando JK, Song W, Ulland TK, Gilfillan S, Colonna M. IL-15 sustains IL-7R-independent ILC2 and ILC3 development. Nat Commun. 2017;8: 14601.
48. Venkateshaiah SU, Zhu X, Rajavelu P, Niranjan R, Manohar M, Verma AK, Lasky JA, Mishra A. Regulatory effects of IL-15 on allergen-induced airway obstruction. The Journal of Allergy and Clinical Immunology. 2018;141:906.
49. Skariah N, James OJ, Swamy M. Signalling mechanisms driving homeostatic and inflammatory effects of interleukin-15 on tissue lymphocytes. Discovery Immunology. 2024;3:kyae002.
50. Wisniewski JA, Muehling LM, Eccles JD, Capaldo BJ, Agrawal R, Shirley D-A, Patrie JT, Workman LJ, Schuyler AJ, Lawrence MG, et al. TH1 signatures are present in the lower airways of children with severe asthma, regardless of allergic status. The Journal of Allergy and Clinical Immunology. 2018;141:141.

Publisher's Note